Inhibition of Parasitic Farnesyl Diphosphate Synthase: Structural and Thermodynamic Studies

by

Srinivas Aripirala

A thesis submitted to Johns Hopkins University in conformity with the requirements for the degree of Doctor of Philosophy

Baltimore, Maryland

February 14, 2014

Abstract

Farnesyl diphosphate synthase (FPPS) is an essential enzyme involved in the biosynthesis of sterols (cholesterol in humans, and ergosterol in yeasts, fungi and trypanosomatid parasites) as well as in protein prenylation. It is inhibited by bisphosphonates, a class of drugs used in humans to treat diverse bone-related diseases. Development of bisphosphonates as anti-parasitic compounds targeting ergosterol biosynthesis has become an important route for therapeutic intervention. As part of my doctoral studies, I determined the X-ray crystallographic structures of complexes of the FPPS from *Leishmania major* (the causative agent of cutaneous leishmaniasis) with three bisphosphonates, at resolutions of 1.8 Å, 1.9 Å and 2.3 Å. Two of the inhibitors, 1-(2-hydroxy-2,2-bis-phosphono-ethyl)-3-phenyl-pyridinium (300B) and 1-(2,2-bis-phosphono-ethyl)-3-butyl-pyridinium (476A), co-crystallize with the homoallylic substrate, isopentenyl diphosphate (IPP), and 3 Ca^{2+} ions. A third inhibitor 3-fluoro-l-(2-hydroxy-2,2-bis-phosphono-ethyI)-pyridinium (46I), was found to bind two Mg^{2+} ions but not IPP. Calorimetric studies showed that binding of the inhibitors is entropically driven. Comparison of the structures of LmFPPS and human FPPS provides new information for the design of bisphosphonates that will be more specific for LmFPPS inhibition. The structure of the LmFPPS-46I homodimer shows that binding of the allylic substrate to both monomers of the dimer results in an asymmetric dimer with one open and one closed homoallylic site. We propose that IPP binds first to the open site that then closes, opening the site on the other monomer that closes after binding the second IPP leading to the symmetric, fully occupied FPPS dimer observed in other structures.

Linear 2-alkylaminoethyl-1,1-bisphosphonates are effective agents against proliferation of *Trypanosoma cruzi*--the etiologic agent of American trypanosomiasis (Chagas disease)-- exhibiting IC_{50} values in the nanomolar range against the parasites. This activity is associated with inhibition at the low nanomolar level of the *T. cruzi* farnesyl diphosphate synthase (TcFPPS). X-ray structures and thermodynamic data of the complexes TcFPPS with five compounds of this family show that the inhibitors bind to the allylic site of the enzyme with their alkyl chain occupying the cavity that binds the isoprenoid chain of the substrate. The compounds bind to TcFPPS with unfavorable enthalpy compensated by a favorable entropy that results from a delicate balance between two opposing effects: the loss of conformational entropy due to freezing of single bond rotations, and the favorable burial of the hydrophobic alkyl chains. The data suggest that introduction of strategically placed double bonds and methyl branches should increase affinity substantially.

Advisor and first reader: Mario L. Amzel, Ph.D.

Second reader: Sandra B. Gabelli, Ph.D.

Acknowledgements

I would never have been able to finish my dissertation without guidance from my committee members, help from friends, and support from my family.

I would like to express my deepest gratitude to my advisor, Dr. Mario Amzel, for his excellent guidance, care, patience, and for providing me with a fertile atmosphere for doing research. I would like to especially thank him for letting me learn the experimental aspects of my research even though I didn't have the background for it. I appreciate the fact that he patiently corrected my writing and navigated me through difficult situations.

I would also like to thank Dr. Sandra Gabelli for guiding my research for the past several years and helping me develop my background in X ray Crystallography, biochemistry, and infectious diseases. Sandra was not only tolerant of my missteps but also gave constructive feedback, which helped me greatly through the course of my research. The good advice, support and friendship of Sandra, has been invaluable both at an academic and a personal level, for which I am extremely indebted to her. I hope I can be as lively, enthusiastic and energetic as Sandra.

I would like to thank my thesis committee Dr. Dan Leahy, Dr. Jurgen Bosch, Dr. Sandra Gabelli, Dr. Sean Prigge, Dr. Terry Shapiro and Dr. Mario Amzel for making it easy for me by setting short-term goals without losing sight of long-term vision. Their invaluable timely advice and support were instrumental in my completion of the doctoral studies. I couldn't have hoped for a better committee.

I would like to thank all the administrative staff in the Biophysics and Biochemical department, who tirelessly helped me in the background with all the paperwork, which is

beyond my comprehension. Special mention to Tammy and Kathy, who always supported me thus helping me stay ahead of time.

I would like to thank Dr. Bertrand Garcia-Moreno for giving me an opportunity by selecting me as a PhD candidate and reposing faith in me in the times of need. I would also thank IMMBI program and Dr. Mario Amzel for their financial support throughout my doctoral studies.

I would like to thank my dear friend Anita Ghosh who was always willing to help me and guide me to the best of her abilities. It would have been a lonely lab without her. Many thanks to Andres Hernandez and Saif Al Qassim for those wonderful discussions about soccer, which I will sorely miss. I thoroughly enjoyed the witty remarks of Oliver who brought joy with his unique sense of humor. I would like to thank Akunna for all the good times we had when we had to share a bench for a good one year. I would like to thank the rest of my lab members for the encouragement given to me during my stay.

I would like to thank my IMMBI friends Sheil, Eva, Tural and Ignacia. I couldn't have asked for better set of classmates. Especially Tural and Sheil have been family to me away from home. I will sorely miss my soccer days with Tural and unending potluck nights with Sheil, Eva and Ignacia. My stay in Baltimore wouldn't have been the same without you guys.

I would like to thank my dear friends Sarita, Saamrat, Abdul, Balaji, Venkat and Sarat for all the good times which included cooking adventures followed by poker nights, exciting Virginia trips, mind numbing telugu movies and memorable dosa days. No words can describe the unconditional love I got from them. They were the single most important

reason why I fell in love with Baltimore. I will cherish all those wonderful memories for the rest of my life. Love you all. You have been my family outside India.

I would like to thank my dear friend Payel for the support she provided and the sacrifices she made for me. I could never have gotten to this stage of my life if not for her constant encouragement. Thank you for everything.

I would like to thank Pankaj Kathuria, Anita Kathuria and Tania Kathuria for their love, support and encouragement. No words can describe the admiration I have for them. They have been a constant source of strength. I am lucky to have you in my life.

Finally I would like to thank my father Rambabu Aripirala and my mother Geetha Aripirala for all the love and support. I would never have been what I am today if not for all their sacrifices. I also thank my dear brother Santosh and Shilpa who have not only stood by me through difficult times, but also provided me with abundance of love and joy. All put together I feel I have the most loving, caring and supportive family. I feel blessed.

Table of Contents

List of tables

List of figures

1. Introduction

Neglected diseases are diseases of poor living conditions and health care inequities [1]. Although they account for nearly half the disease burden in developing countries, investments in research and development of new drugs, have not prioritized this area [2]. Among the most neglected maladies, Chagas disease, Sleeping sickness, Malaria, Leishmaniasis and Toxoplasmosis, are the most important since they affect thousands of people every year with high morbidity [3, 4].

Besides insufficient funding for research related to neglected diseases, the results are seldom translated into therapeutic advances, such as new drugs, vaccines or diagnostic methods. One reason for this situation is the low market potential payoff for the pharmaceutical industry because the affected population has very low income and present mostly in developing countries [5]. Chemotherapy has an important role not only in the treatment of patients but also in reducing the transmission of parasitic infections. There has been limited commercial interest in developing improved therapeutics for these diseases even though existing treatments are of limited effectiveness and often highly toxic [6, 7].

Drug discovery is a long drawn and complex process, starting with the discovery of a novel therapeutic target and ending with the finding of an effective clinical candidate, spanning several years. This process requires synthesis and evaluation of multiple lead compounds for both their potency against targets and side affects on the off-targets. Repurposing drugs that are already approved has a huge advantage over the discovery of

the new compounds if it can quickly advance into later stage clinical trials in the patient population to assess efficacy [8].

1.1 Parasites and their diseases

Protozoan parasites belong to four distinct groups: amoebae, flagellates, ciliates and sporozoan. They are all single-celled organisms that replicate in the host spreading the infection rapidly. Among the many neglected diseases caused by protozoan parasites, I worked with enzymes belonging to two parasitic species: *Leishmania major* and *Trypanosoma cruzi*. As part of my doctoral studies, I characterized the interactions between a promising class of drugs, bisphosphonates, and their target, FPPS.

1.1.1 *Leishmania* species: Leishmaniasis

Leishmaniasis, a parasitic disease caused by any one of the 20 species of eukaryotic organisms of the genus Leishmania. The disease exists in three forms: cutaneous (CL), visceral (VL) and mucocutaneous (ML). CL, caused by L. major and L. mexicana, is predominantly found in Saudi Arabia, Iran, Afghanistan, Pakistan, Peru and Brazil, where it affects twelve million people with 1.5 million new cases being reported annually. The most severe form is visceral leishmaniasis (also known as *kala azar* or black fever) caused by *L. donovani* and *L. infantum*, in which the parasites cause hepatosplenomegaly, fever, weight loss and anaemia [9-12]. VL affects people in Bangladesh, India, Nepal, Sudan and Brazil. Incubation period can vary and may reach two years, and if left untreated, the disease is fatal in 100% of cases. Leishmaniasis is endemic in 88 countries with 350 million people at risk [9-12]. There are more than 12

million infected with 2 million new cases of the cutaneous form and half million new cases of the visceral form occurring each year. Visceral form of leishmaniasis is estimated to have caused more than 50,000 deaths worldwide annually. The disease is transmitted through the bite of infected sand flies of the genera Phlebotomus and Lutzomyia, which are the most common vectors in the Old and New World respectively. Leishmaniasis is mainly a zoonotic disease (with reservoirs in rodents and canines), but, in Africa and in the Indian subcontinent visceral leishmaniasis, caused by Leishmania donovani, is an anthroponotic disease transmitted from human-to-human by sandflies [9, 12].

Leishmania parasites occur in two different forms, extracellular promastigotes (infectious form) in the sandfly vector, and intracellular amastigotes (replicative form) within the phagolysosomes of human host macrophages, which is the stage responsible for the leishmaniasis pathology (Fig. 1). Parasites in this genus are classified into two subgenera according to the region of the sandfly gut where colonization and development occur: mid and foregut development *Leishmania* (Leishmania) and *Leishmania* (Viannia) hind gut [13-16].

Current drug treatments of visceral leishmaniasis suffer from host toxicity, high cost, difficulty to administer and drug-resistance development. Pentavalent antimonials have been the first-line drugs in the treatment of visceral leishmaniasis for more than 70 years, except in India due to the extensive development of resistance [9, 14, 16-21]. The antifungal drug amphotericin B has become the second-line treatment of visceral leishmaniasis, in spite its severe and potentially lethal side effects [19-21]. Lipid formulations of amphotericin B with reduced toxicity have been developed and are now

the choice of treatment for visceral leishmaniasis in developed countries [19-21]. But, due to high cost, this treatment is not an option in most of the countries with endemic disease. Although drugs such as miltefosine and paromomycin are in the pipeline with promising therapeutic effects, [9, 16, 19-21] unfortunately, they also suffer from limitations such as prohibitive cost, toxicity, challenging administration route, lengthy treatment schedule and the generation of drug resistance.

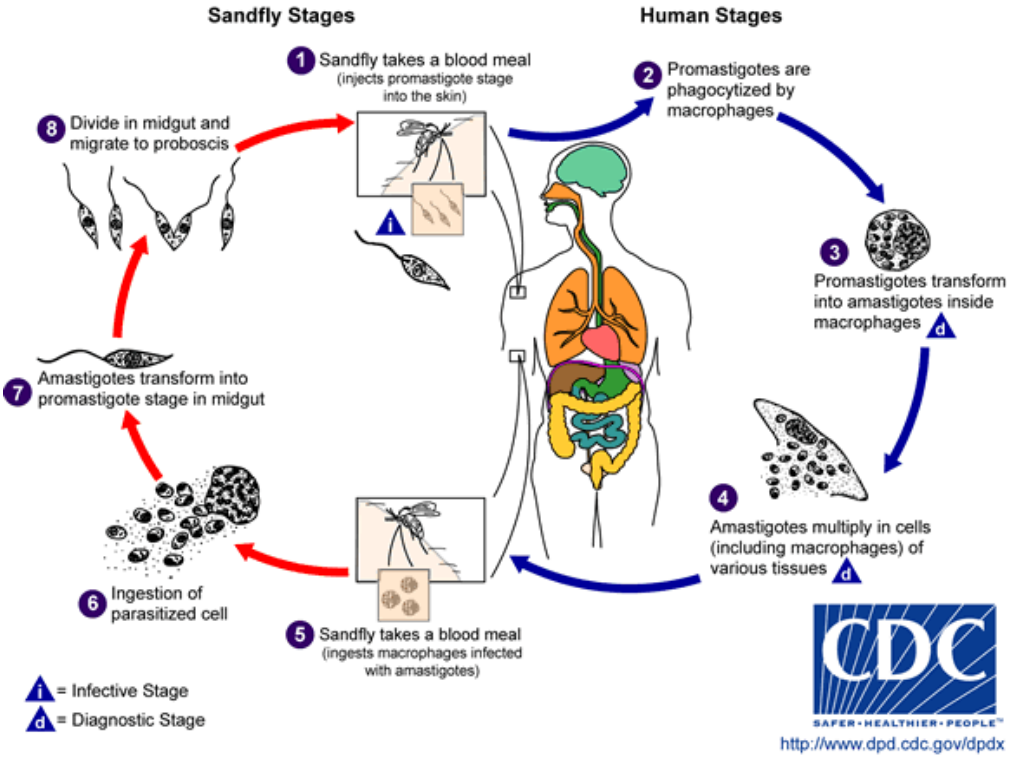

Figure 1. Life cycle of Leishmania parasite.

reproduced from: http://www.dpd.cdc.gov/dpdx

1.1.1 Trypanosoma cruzi: Chagas disease

American trypanosomiasis, Chagas disease, is a devastating and potentially life-threatening illness caused by infection with *Trypanosoma cruzi*. It is endemic and widespread in Latin America, with 11 million chronically infected individuals mainly residing in abject poverty in rural areas. It is estimated that 100 million people are at risk with 14,000 deaths occurring annually [9, 22]. Recently, the disease has spread to other continents such as Europe and USA due to immigration of population initiating a "globalization" of Chagas disease [23, 24]. The parasite is most often transmitted to humans by the infected faeces of 'kissing bugs' (mainly by species belonging to the *Triatoma*, *Rhodnius* and *Panstrongylus* genera). The bugs hide in cracked walls of adobe houses and come out at night to suck blood. Reservoirs of parasites are present both in wild and domestic animals. An individual can also become infected with *Trypanosoma cruzi* through contaminated food [25-27], blood transfusion [28], organ transplantation [29], vertical transmission (passed from an infected mother to her child during pregnancy or birth) [30] or accidental injection [31].

The *Trypanosoma cruzi* life cycle involves stages in reduviid insect vectors and in mammalian hosts. In the gut of the vector epimastigotes replicate and differentiate into metacyclic trypomastigotes, the infective form of the parasite, which are transmitted to the mammalian host. Trypomastigotes enter the host bloodstream and ultimately invade a variety of cell types (including cardiac muscle cells) where they undergo differentiation into the amastigote form. Intracellular amastigotes differentiate into trypomastigotes that are released into the blood and invade other cells or are ingested by the vector during a blood meal, continuing the cycle (Fig. 2) [13].

Existing treatments for the Chagas disease is not only lacking in efficacy but also fraught with side affects. Benznidazole and Nifurtimox are the only drugs available against Chagas disease. Although almost 100**%** effective if given soon after infection, these drugs cause adverse reactions in up to 40**%** of treated patients, and are ineffective against the chronic form of the disease. Therefore there is a pressing need for new and better drugs. One problem to consider when designing new drugs against *Trypanosoma cruzi* is that these parasites circulate in the blood in high numbers only during the initial acute phase. During the chronic phase, which is thus far incurable, the parasites reside intracellularly, mainly in the heart muscle and in the smooth muscle of the digestive tract [9, 13, 22, 32].

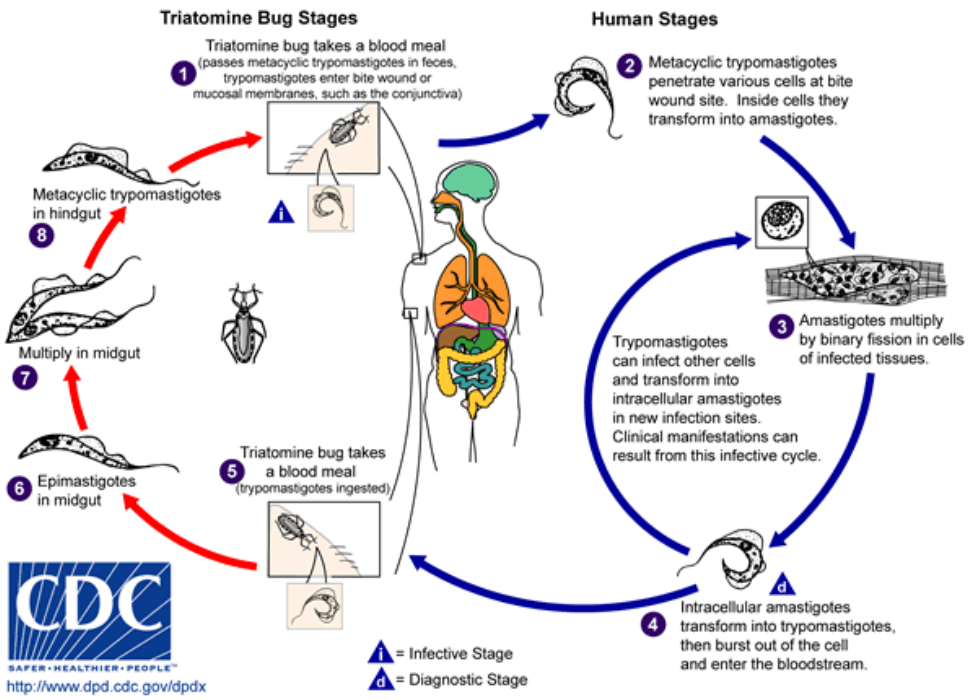

Figure 2. Life cycle of Trypanasoma cruzi parasite.

reproduced from: http://www.dpd.cdc.gov/dpdx

1.2 Farnesyl Diphosphate Synthase

Farnesyl pyrophosphate synthase (FPPS) is one of the key enzymes of the mevalonate pathway. It catalyzes the committed step in the generation of isoprenoid lipids utilized in sterol synthesis and the post-translational modification of proteins essential for cell function. Some of these prenylated proteins including Ras and other G-proteins are involved in signal-transduction pathways and are indispensable for the survival of protozoan parasites[33]. In humans, FPPS is the target of bisphosphonates[34].

Bisphosphonates that block the formation of intermediates along the isoprenoid precursor biosynthesis were investigated as possible antiparasitic agents [35], and it was

found that they inhibit several non-mammalian species, including protozoan parasites [36, 37].

FPPS inhibitors are being used in humans for treating a number of diseases, including bone-related disorders characterized by excessive bone resorption, such as osteoporosis, and cancer metastasis to bone [34, 38]. These same inhibitors were shown to be effective *in vivo* and *in vitro*, against infectious diseases caused by *Leishmania donovani*[39], *Toxoplasma gondii*[40], *Trypanosoma brucei*[41], *Trypanosoma cruzi*[42, 43] and *Plasmodium falciparum*[44] opening the way for new therapeutic applications of existing FPPS inhibitors. These uses are becoming an area of significant patent activity, demonstrating growing recognition of the versatility and underdeveloped potential of these drugs [38].

1.2.1 Mechanism

Poulter et. al. have established that the mechanism of FPPS involves a ionization-condensation-elimination. They were able to differentiate between the competitive displacement mechanisms by substituting hydrogen with the powerful electron withdrawing fluorine in the allylic substrate. Kinetic studies with this modified analog resulted in no effect on K_m. However, the rate of condensation was reduced 1000-fold with respect to that of the normal reaction[45, 46].

Later Laskovics et. al. determined that binding follows an ordered sequential mechanism with the allylic substrates DMAPP or GPP binding first and then binding of the homoallylic substrate IPP[47]. Their work also indicates that GPP leaves the active site after the first condensation reaction before it reenters for the second 1'-4

condensation reaction to form the final product FPP. The rate-limiting step at steady state is the isomerization of E.Mg^{2+}-FPP.Mg-PPi or release of products. The following is the summary of the mechanism:

1) The allylic substrate DMAPP enters the active site along with divalent cations

2) Following a conformational change, the homoallylic substrate IPP enters

3) After the first of the two consecutive condensation reactions GPP leaves the active site before it re-enters again

4) FPPS catalyzes a second 1'-4 condensation of GPP and IPP to give the final product FPP

1.2.2 Site-Directed Mutational Studies on the Catalytic Residues in FPPS

Sequence alignment of the sequences of the FPPS enzyme from various bacterial species identify 5 major conserved regions: First Aspartate Rich Motif (FARM: residues 98-102 in LmFPPS: DDXXD), Second Aspartate Rich Motif (SARM: residues 250-254: DDXXD), Residues 107-109 RRG, conserved Lysine 254 and basic C terminal. Various groups have carried out site-directed mutational studies to determine the effects of substitutions at these positions on the kinetic parameters. Song et. al. determined that mutants D100A, D101A and D104A of the FARM in yeast species, had only 10^{-5} to 10^{-6} of the activity of the wild type[48]. In the same study they also showed that the mutations D240A and D241A (SARM) drastically reduced the catalytic activity while the D244A mutant reduced k_{cat} by 16-fold and increased K_m (IPP) by 5-fold and Km (GPP) by 2-fold.

In another study Marrero et. al. showed that FPPS mutation D243E in rat liver decreased V_{max} by 90-fold while mutant D247E (DDYLE) had the same k_{cat} as the wild-type, indicating that it may not be involved in catalytic activity[46]. These studies combined with the structural studies indicate that the carboxylate moieties of the aspartate residues play a vital role in enzyme's catalytic activity.

Linsheng et. al. showed that FPPS mutants R109Q and R110Q in yeast reduced the catalytic activity by a factor of 10^6. In another study, Alison Joly et. al. showed that the mutants R112K and R113K in rat FPPS decreased k_{cat} 1000-fold[49]. However these mutants had no impact on K_m for IPP or GPP. Our structural studies with Leishmania FPPS in complex with the bisphosphonate 300B, IPP and Ca^{2+} ions revealed interactions between the corresponding arginine residues (R108, R109) and the phosphate moieties of the bisphosphonates.

The role of a conserved lysine residue Lys254 in LmFPPS found in the loop following SARM is unclear. Mutant K254A had no effect on K_m of either substrate and reduces k_{cat} modestly by a factor of 7. Structural studies done in our lab show different conformations lysine adopted in the presence and absence of IPP. This lysine interacts with the phosphate moiety of the allylic substrate when IPP binds.

Mutational studies done by Koyama *et. al*. on another conserved region VI (Sequence alignment) showed that the mutants F220A and Q221E displayed 10^5 and 10^3 reduction in the catalytic activity of the FPPS from *B. Stearothermophilus*[50]. Structural studies in the Leishmania FPPS reveal that Phe220 stabilizes IPP. The large decrease in

the k_{cat} for the F220A mutant indicates that this Phe is involved in catalysis. They suggest that it may be involved in stabilizing the carbocation through cation π-interactions.

The final region of significance is the C-terminal, which has a high proportion of basic amino acids. Among these conserved basic amino acids, mutational studies were carried out on Arg295 of the FPPS of *B. Stearothermophilus*. The mutant R295V displayed a k_{cat} similar to the wild type but showed a 3-fold increase in K_m for IPP suggesting that the C-terminal is involved in the binding of IPP.

2. Results and Discussion

2.1 Structural and thermodynamic basis of the inhibition of *Leishmania major* Farnesyl Diphosphate Synthase by nitrogen containing bisphosphonates

Sections previously submitted as:

Structural and thermodynamic basis of the inhibition of *Leishmania major* Farnesyl Diphosphate Synthase by nitrogen containing bisphosphonates.

Acta Crystallography D, 2013

Recent studies show that bisphosphonates such as pamidronate and risedronate, drugs used in humans in the treatment of osteoporosis[51, 52], are effective against the *Leishmania* parasite both *in vitro* and *in vivo*[53, 54]. These bisphosphonates target farnesyl diphosphate synthase (FPPS). The shortcomings of the drugs being used for the treatment of Leishmaniasis point to a critical need for finding new therapeutic compounds. Bisphosphonates are ideal candidates for developing new, more effective drugs against *Leishmania* parasites because of their proven safety in humans. Since the sequence identity among the FPPS of *L. major, L. infantum, L. donovani* and *L. mexicana* is greater than 90% it may be possible to design compounds that inhibit this enzyme in all *Leishmania* strains. In this section, we report thermodynamic data of four nitrogen-containing bisphosphonate inhibitors binding to *L. major* FPPS (LmFPPS) as well as the structure of three of these complexes (Fig. 3). The structures show that while LmFPPS is structurally similar to human FPPS, differences in the catalytic pocket identified in this work should open the way for the design of parasite-specific inhibitors. The thermodynamic footprint of binding of these inhibitors to LmFPPS, determined by isothermal titration calorimetry (ITC), provides additional clues for inhibitor design. In addition, the structure of the complex of LmFPPS with the bisphosphonate 3-fluoro-l-(2-hydroxy-2,2-bis-phosphono-ethyl)-pyridinium (46I) provides the structural insights into the ordered sequential mechanism proposed by Laskovics and Poulter[47]. In this structure with the two allylic sites occupied, the two empty IPP sites adopt different conformations, one open and one closed, suggesting an alternating site mechanism for binding of the homoallylic substrate.

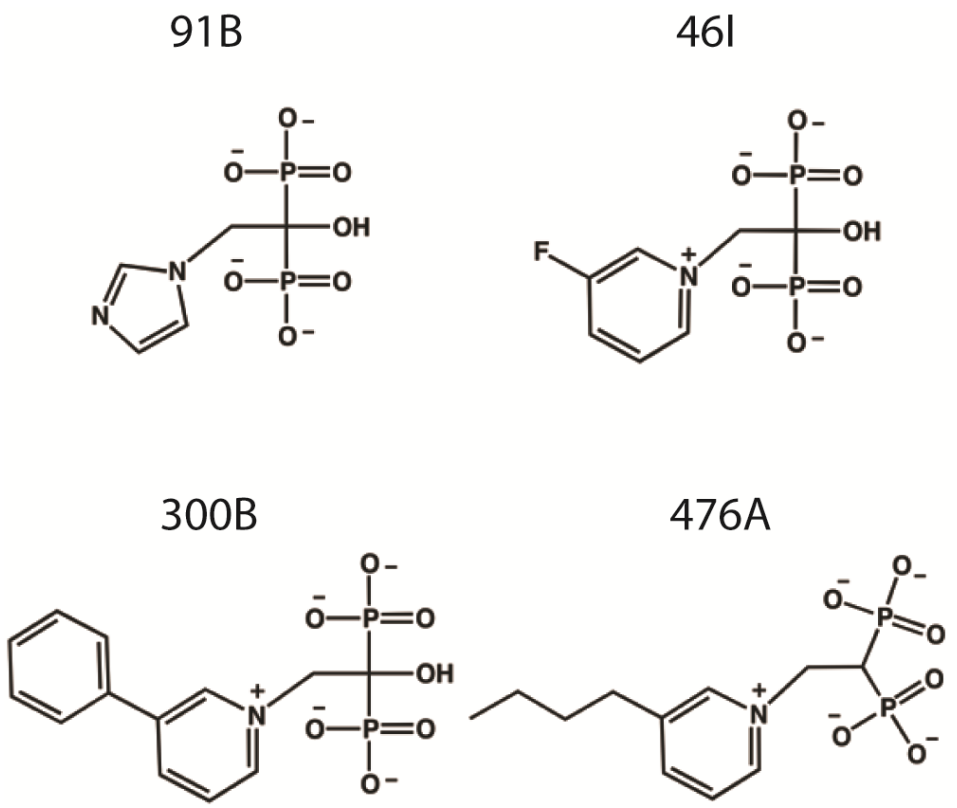

Figure 3. Bisphosphonates used in this study.

2.1.1 Overall Structure of LmFPPS Complexes

The structures of the complexes of LmFPPS with three bisphosphonate inhibitors 300B, 476A and 46I were determined by x-ray diffraction at resolution of 1.8 Å, 1.9 Å and 2.3 Å respectively. The structures of 300B and 476A also contain the homoallylic substrate IPP and three Ca^{2+} ions, and that of 46I contains two Mg^{2+} ions but no IPP (Table 1). LmFPPS is a homo-dimer similar to those of FPPS from other species[7, 55, 56] (Fig. 4a,b). Formation of the dimer buries 5770 A^2 of accessible surface area. The monomers have the typical FPPS fold: a ten-helix bundle with four additional helices running perpendicular to the bundle. The two substrate sites, allylic and homoallylic, are part of a large connected cavity at the "top" of the helix bundle. In the structures of the complexes, the inhibitors occupy the allylic site and the IPP, when present, the homoallylic site (Fig. 4c). Three divalent cations and the side-chains of aspartate residues from two aspartate rich motifs (DDXXD; residues 98-102 in the first aspartate and residues 250-254 in the second aspartate rich motif) coordinate the bisphosphonate atoms of the inhibitors bound at the allylic site[7, 57, 58]. The divalent cations at the active site are octahedrally coordinated with water molecules and the oxygen atoms of the bisphosphonates[13,24,25]. In the structures reported here, the three divalent cations in the structures of LmFPPS-300B-IPP and LmFPPS-476A-IPP were determined to be Ca^{2+}, using anomalous scattering data (Fig. 4d). Although Mg^{2+} is probably the physiological cation[57], Ca^{2+} from the crystallization solution is present in these crystals.

Table 1. Structures of LmFPPS complexes: Data collection and Refinement Statistics.

Crystal	LmFPPS-476A-IPP-Ca^{2+}	LmFPPS-300B-IPP-Ca^{2+}	LmFPPS-46I-Mg^{2+}
Space group		$P2_12_12_1$	
Cell dimensions (Å)	a = 80.3	a = 80.4	a=60.2
	b = 85.7	b = 86.0	b=143.7
	c = 106.7	c = 107.1	c=194.3
	α=b=γ = 90°	α=b=γ = 90°	α=b=γ = 90°
X-ray Source	FR-E/Raxis IV	FR-E/Raxis IV	Beam line 31-b APS
Res(Å)	50.0-1.8	50.0-1.9	50.0-2.3
(HighRes shell)	(1.86-1.80)	(1.97-1.90)	(2.38-2.30)
Measured Reflections	469,090	400,007	384,740
Unique Reflections	68,699	58,810	69,237
I/σ	36.6 (2.4)	32.5 (2.9)	34.2(3.3)
Completeness (%)	99.8 (99.9)	99.4 (95.3)	91.2(96.5)
R_{merge} (%)	7.0 (54.5)	7.2 (47.3)	10.6(67.5)
		Refinement	
R_{cryst} (%)	17.8	17.2	22.7
R_{free}	22.9	21.3	28.4
Monomer in ASU	2	2	4
Protein atoms	5786	5808	11,474
Water molecules	693	678	294
		R. M. S. deviations	
Bond length (Å)	0.008	0.010	0.009
Angle (°)	1.1	1.2	1.6
B-factor($Å^2$)			
Protein	26.7	22.0	45.5
Ligand	25.2	19.7	73.8
H_20	36.5	31.9	42.4

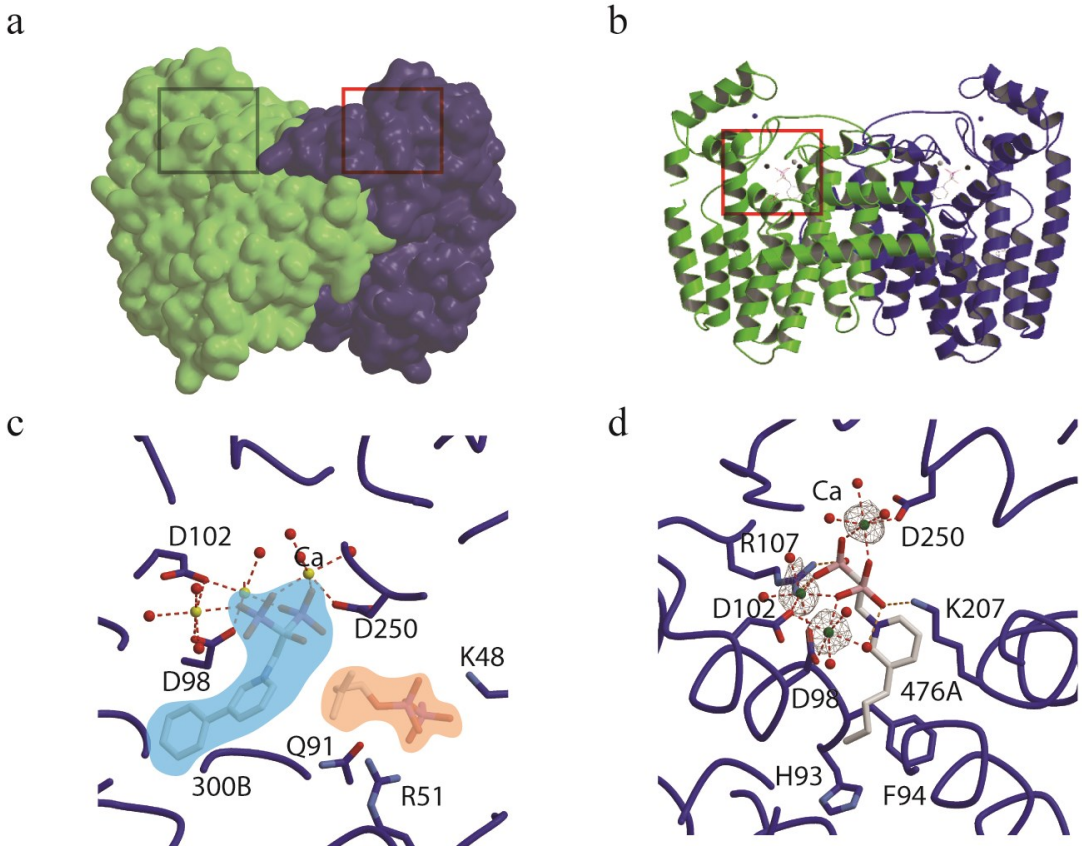

Figure 4. Structural features of the active site of LmFPPS.

(a) Surface representation of the complex with 300B, IPP and three divalent cations. The two boxes show the active site in each of the two monomers. (b) Ribbon representation of the complex. 300B and IPP are shown as stick models while divalent cations Ca^{2+}, are shown as spheres. The box shows the active site in one of the monomers. (c) Octahedral coordination of the Ca^{2+} is shown as red dashed lines. Water molecules are shown as red spheres and Ca^{2+} ions as yellow spheres. Protein backbone and the residues in the active site are shown in blue. 300B and IPP are shown as a stick models in white. The blue shaded region highlights the allylic site while the homoallylic site is shown as an orange shaded region. (d) LmFPPS in complex with 476A, IPP and 3 Ca^{2+}. Divalent cations were determined to be Ca^{2+} using anomalous scattering data measured at the wavelength corresponding to the Ca edge. Water molecules are shown as red spheres and Ca^{2+} ions in green. Protein backbone and the residues in the active site are shown in blue. 476A is shown as a stick model in white. Residues from the first and second aspartate rich regions are shown coordinating Ca^{2+} ions. Density shown around the Ca^{2+} was calculated using anomalous scattering data.

2.1.2 Interactions of 300B and 476A with LmFPPS

The bisphosphonate moieties of both 300B and 476A interact with residues in the active site in a similar manner (Fig. 5a, b). Their phosphonate moieties accept H-bonds from the amino groups of Lys207, Lys264 and the guanidinium of Arg107 and interact indirectly through Ca^{2+} or water molecules with the carboxylates of Asp98, Asp102 and Asp250. The carboxylate of Asp99, at hydrogen bonding distance of the Nε and the Nη2 of Arg107, positions Arg107 to interact with the phosphate of the inhibitor. Deeper into the active site, Leu95, Met101 and Phe94 interact with either the alkyl chain of 476A or the benzene ring of 300B. The side chain of Gln167, at the end of the active site, is in a different conformation in the two structures: it rotates approximately 20° (χ2) to accommodate 300B, the bulkier ligand (Fig. 5c). His93, thought to be involved in determining the product length[59], is in the same conformation in both complexes (Fig. 5c).

The hydroxyl group at the C1-position of 300B makes a hydrogen bond with Asp250 (distance 2.9 Å). In contrast to the structure of the *Trypanosoma cruzi* FPPS where the presence of the C1-OH causes disordering of IPP in the active site[6], the IPP in the structure of LmFPPS with 300B is well ordered (average temperature factor of 21.75 $Å^2$).

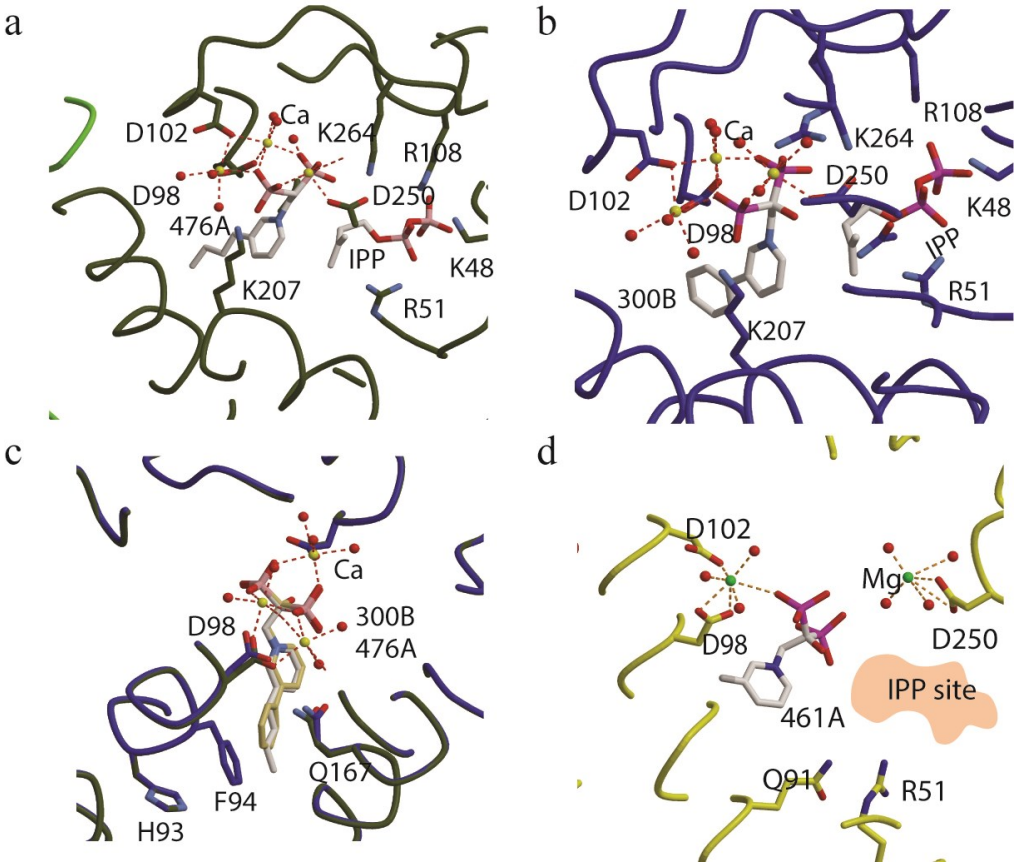

Figure 5. Active site of LmFPPS in complex with bisphosphonates.

(a) LmFPPS in complex with 476A, IPP and 3 divalent cations. Water molecules are shown as red spheres and Ca^{2+} in yellow. Protein backbone and the residues in the active site are shown in dark green. 476A and IPP are shown in white as a stick model. Residues from the first and second aspartate rich motifs are shown coordinating Ca^{2+}. Basic amino acids Arg108, Arg51 and Lys48 are observed interacting with the diphosphate moiety of IPP. (b) Active site of LmFPPS in complex with 300B (white, stick representation), 3 Ca^{2+} (yellow, spheres) ions and IPP (white, stick representation) and figure is a close up; shown in the same orientation as in 3a. (c) Structural alignment of LmFPPS-300B-IPP-Ca complex (green) with the LmFPPS-476A-IPP-Ca complex (blue). Residues Asp98, Asp102 and Asp250 that participate in the ion/bisphosphonate coordination overlapped without any conformational difference. Gln167 (red arrow) in the 300B complex (blue) rotates 20° ($\chi 2$) to accommodate the bulkier ligand, 300B. (d) Active site of LmFPPS in complex with 46I (white, stick model), 2 Mg^{2+} ions (green spheres) are shown in the same orientation as in 3a. The orange shaded region shows the empty IPP site.

2.1.3 Interaction of 46I with LmFPPS

Although the complex of LmFPPS with 46I crystallizes in the same $P2_12_12_1$ space group as the other two complexes, its crystals are not isomorphous with the other two. Unlike the structures of the complexes with 300B and 476A, which have one dimer in the asymmetric unit, the asymmetric unit of the 46I complex contains two dimers. Surprisingly, even though IPP was present in the crystallization buffer there is no density for IPP in the active sites of any of the four monomers (Fig. 5d). Neither sulfate nor phosphate was observed occupying the position of IPP, ions that have been seen to bind to this site in other FPPS structures[55].

46I contains fluorine in the *meta* position of the phenyl group of the side-chain (Fig. 3d). Interactions of the bisphosphonate moiety of 46I with protein residues are similar to those seen with the other two ligands but there is, in addition, a hydrogen bond formed between the fluorine and Glu167. Unlike the other two structures, only two divalent cations (identified as Mg^{2+}) are found in the active site, coordinated by the conserved residues Asp98, Asp102 and Asp250 (Fig. 5d). Also the residues D98 and D102 coordinating the comparable divalent ion in 300B complex are in a different conformation in the 46I complex due to the missing divalent cation. Another difference involves the coordination of one of the ions (Ca^{2+} in the 300B complex, Mg^{2+} in the 46I-complex). This ion shows a complete octahedral coordination in the 300B complex involving D250, water molecules and the allylic substrate 300B. In contrast, in the 46I complex the ion interacts with the ligand 46I indirectly through a water molecule.

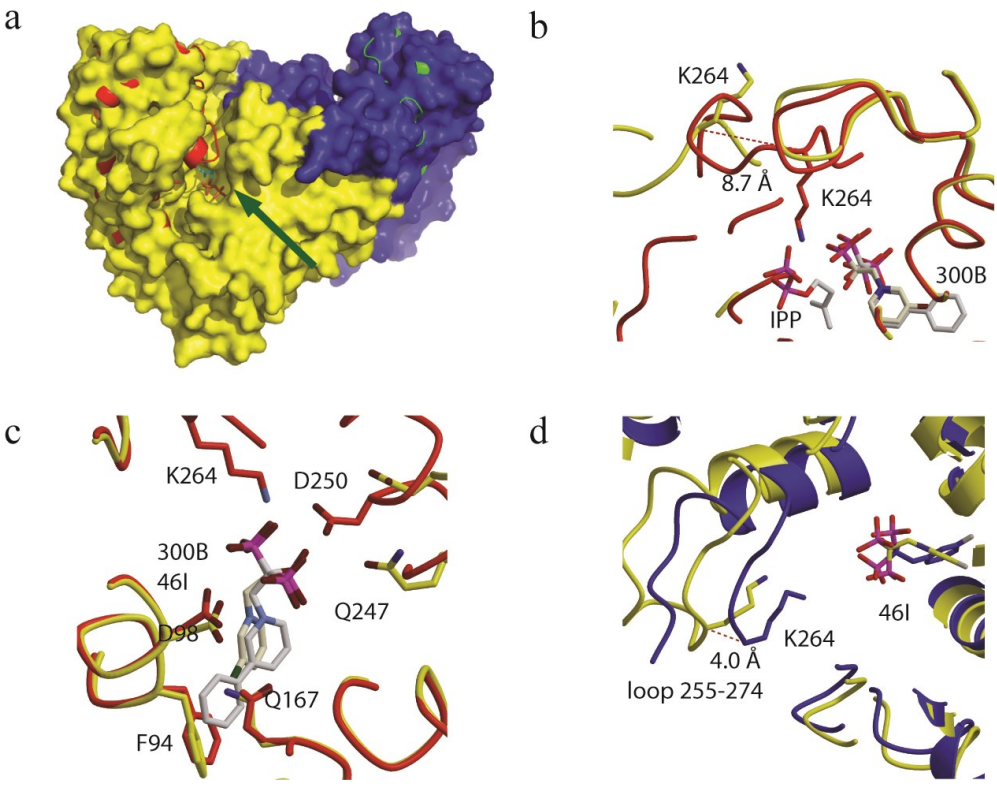

Figure 6. Structural comparisons of the LmFPPS active site in the presence and absence of IPP.

(a) Surface representation of the complex with 46I and divalent cations (yellow and blue) overlapped on the LmFPPS in complex with 300B, IPP and three divalent cations (red and green ribbon representation). Green arrow points to the cleft (opening) in the LmFPPS-46I-Mg complex in the absence of IPP. (b) Zoomed-in detail of Figure 6a around the helix and the loop containing residues 255 to 274. Conserved residue Lys264 is seen interacting with the phosphate moiety of the allylic ligand (300B) in the closed conformation. In the LmFPPS-46I-Mg complex (yellow) in which the loop adopts the partially open conformation, Lys264 is 8.7 Å further away from corresponding residue in 300B complex (blue). (c) Structural overlap of LmFPPS in the complexes with 300B (red) and with 46I (yellow). Residues of the allylic site that have different conformations are shown. The inhibitor bound in each complex is shown. Metals are not shown for clarity. (d) Structural comparison of the monomers A and B of LmFPPS in complex with 46I. In the region around helix containing second aspartate rich motif and the loop 255-274, the conserved residue Lys264 is 4 Å further away from the allylic substrate in chain B than in chain A.

2.1.4 Structural effects of IPP binding

The presence of IPP in the 300B structure, bound by residues Phe246, Arg108 and Lys264, introduces significant structural changes compared to the 46I complex. The loop that follows the second aspartate rich region (residues 255 to 274) is in a different conformation in the two structures (Fig. 6a): it is displaced up to 8.7 Å in the 46I complex (Fig. 6b). The closed conformation of the 300B complex is a direct result of the interactions of the protein with IPP. For example, closing of the loop due to the presence of IPP, brings Lys264, of the loop to interact directly with 300B(Fig. 6b).

2.1.5 Asymmetry in the LmFPPS-46I complex homodimers

The four monomers (A, B, C and D) in the asymmetric unit of the 46I complex crystal are organized into two dimers (AB and CD; rmsd 0.56 Å) but within each dimer the monomers show significant differences (rmsd: 1.4 Å), localized in the loop containing residues 255-274. For example residue Lys264 of monomer A is 5.6 Å away from the closest bisphosphonate oxygen but this residue is 8.0 Å away in monomer B (Fig. 6d). Another key difference between the chains of the LmFPPS-46I dimer is in the position of the Mg^{2+} coordinated to Asp250. In monomer B (or D), the helix containing the second aspartate rich motif and the loop following that helix are in a more open conformation as compared to chain A (or C). These changes create a large difference between the two monomers in the accessibility of the homoallylic site (see below).

We propose that the structure observed in the LmFPPS-46I-Mg complex represents a partially open intermediate structure, ready for IPP to enter one of the two

active sites, whereas the LmFPPS-300B-IPP-Ca and LmFPPS-476A-IPP-Ca complexes adopt the closed conformation after both the allylic and the homoallylic sites become occupied.

2.1.6 Cellular Activity of the inhibitors

Leishmania parasites assume different forms during their life cycle[60]. The vectors, blood sucking females of the genus *Phlebotous* and *Lutzonia*, ingest the parasites while feeding on blood of infected individuals. The parasites are released from the ingested macrophages as amastigotes into the stomach of the insect, where they convert into motile flagellated promastigotes. This form undergoes binary fission. Once the sand fly bites a human, the promastigotes get taken in by the macrophages and revert to the amastigote form. Leishmania amastigotes are able to survive the extreme acidic conditions of the macrophages, where they multiply. It is this amastigote form that causes the disease in the human host.

Both 300B and 476A were screened against *L. donovani* strain MHOM/ET/67/L82 and for cytotoxicity against skeletal myoblasts (Table 2). Their *in vitro* activity against the Leishmania parasites was about 20 times less active than the standard-of-care drug, miltefosine. The compounds are about 10-12 times more active against *Trypanosoma brucei*, but less active against *Trypanosoma cruzi,* highlighting the differences in activity against different species. This diversity in activity is also clear from the observation that with *L. mexicana amazonensis*, the bisphosphonate pamidronate produces a parasitological cure in a mouse model of infection, and more

lipophilic bisphosphonates have potent activity against malaria parasites *in vivo*[54]. Macrophage *in vitro* screening showed that the compounds were toxic to the macrophages at 10 μg/mL and were not active at 3.3 μg/mL. At this last concentration, the intracellular parasites appeared shrunken, with a corrugated surface, preventing an assessment of how viable the amastigotes were in the macrophages. Clearly more selectivity against LmFPPS is needed and some clues for possible changes in these compounds are suggested by comparison of the X-ray structures of the human and *Leishmania* proteins.

Table 2. Cell based assay.

Axenic *in vitro* activity against *Leishmania donovani* (and other trypanosomatids) and cytotoxicity towards the L-6 cell line. The IC_{50} values are the mean of two independent assays and vary less than ±50%.

Compound	***Leishmania donovani* IC_{50} μM**	***Trypanosoma brucei* IC_{50} μM**	***Trypanosoma cruzi* IC_{50} μM**	**L-6 IC_{50} μM**
300B	9.8	1.03	81.5	65.2
476A	15.4	0.9	99.3	57.2
Miltefosine	0.5	-	-	-

2.1.7 Comparison of the LmFPPS and HsFPPS structures

In both human and *Lm* enzymes the divalent cations interact with the phosphates of the bisphosphonate, while IPP interacts with residues Lys48 and Arg108 of the enzyme. The residues involved in these interactions are conserved between the human and *L. major* proteins, as well as in the FPPSs of other species (Fig. 7a). This is also true for residues at the bottom of the pocket, where bulky amino acids, Phe94 and His93 in LmFPPS, restrict the length of the allylic product/substrate[61, 62]. In the region of the pocket that recognizes the isoprenoid chain, however, there are small but significant differences between residues of HsFPPS and LmFPPS. For example, an alanine residue that points towards ligand at the bottom of the pocket of HsFPPS (Ala107) is replaced by a glutamate (Glu97) that points away from the ligand in LmFPPS, changing the shape of the pocket available for inhibitor binding. Another difference, the replacement of Leu129 in LmFPPS by Asn133 in HsFPPS at the bottom of the active site, can also potentially be exploited for the design of inhibitors that show specificity for the parasite enzyme (Fig. 7b). For example, a new inhibitor with a methyl added to the distal ring of 300B compound may exploit the differences between the human and Leishmania enzymes (Fig. 7c).

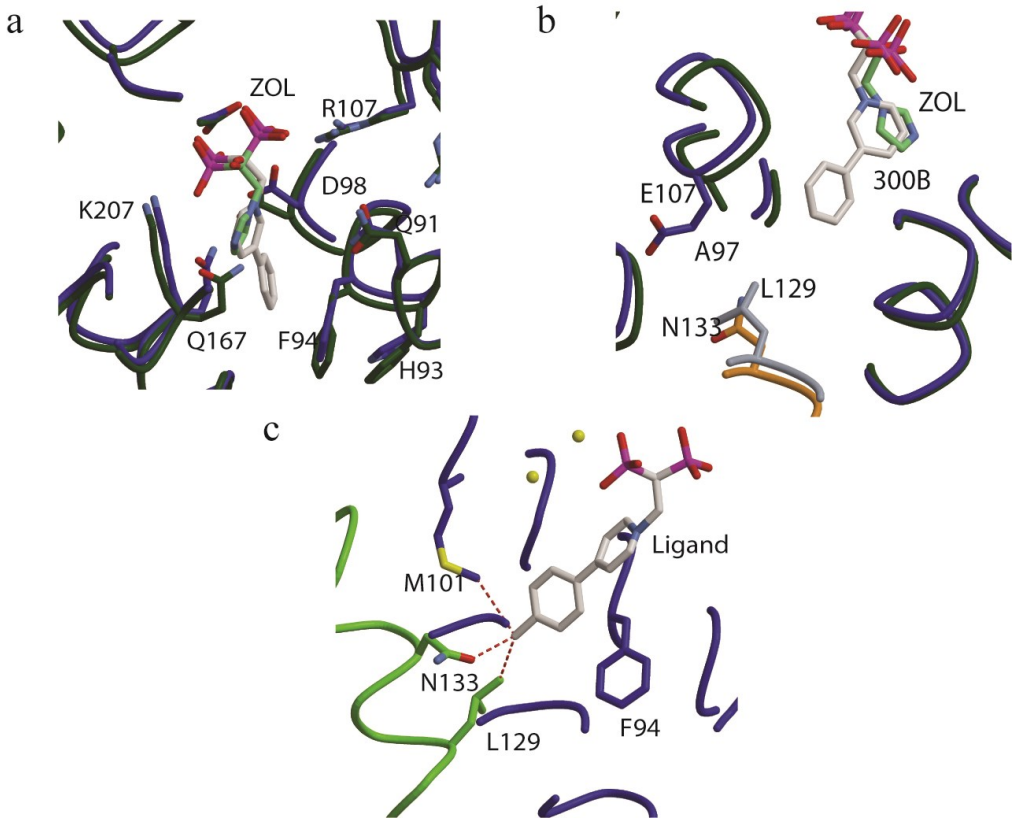

Figure 7. Structural comparisons between the active site of LmFPPS and Human FPPS.

(a) LmFPPS in the 300B complex (blue) and HsFPPS in the zoledronate (Zol, 91B) complex (dark green) are shown in ribbon representation. While, conserved residues His93, Phe94, Asp98, Gln91 and Arg107 (stick models) are in the same conformation, Gln167 in 300B has a different conformation to accommodate the bulkier ligand. The ligands 300B (white) and Zol (light green) are shown as stick models. (b) Deeper in the allylic pocket two residues are different between the two molecules: Glu107 (dark blue, chain A) and Leu129 (light blue, chain B) of LmFPPS are replaced in HsFPPS by Ala97 (green, chain A) and Asn133 (orange, chain B). (c) Allylic site shown with a proposed inhibitor with a methyl group added to 300B. The relation of the methyl group to the nearest residues is shown in red dotted lines. The other monomer of the molecule is shown in green. Residues Leu129 and Asn133 from monomer B are shown as green stick models while Met101 is shown as a blue stick model.

2.1.8 Entropy driven ligand binding

The binding energetics of four inhibitors to LmFPPS: 46I, 300B, 476A and 91B (zoledronate) were measured using Isothermal Titration Calorimetry (ITC). The data show that in all cases binding is entropy driven. The reactions are endothermic ($\Delta H > 0$; Table 3, Fig. 8) with K_ds in the range 28.0 – 342.5 nM. The entropies of binding are in the range of 41.2-45.2 cal/K/mol ($-T\Delta S$ between -12.4 and -13.6 kcal/mol), similar to those reported previously for other cationic side-chain-containing bisphosphonates binding to *T. brucei* FPPS[63]. The smaller ligands 46I and 91B bind more tightly than do the larger ligands, 300B and 476A. Also, 91B binds five-fold less tightly with a K_d of 150 nM to the HsFPPS than to the LmFPPS[58]. In the case of 300B, the reduced affinity results from a binding enthalpy that is more unfavourable than those of the other inhibitors. This may be a consequence of the increased difficulty in accommodating this larger compound within the binding site. Interestingly entropic contribution to the binding of 300B is more favourable than of 476A's binding. We believe this is due to the combination of two forces opposing each other: 1) loss of conformational entropy due to freezing of single bonds in the bisphosphonate, more so in 476A than in 300B. 2) Release of larger number of water molecules, which previously formed a clathrate around the bisphosphonates.

Table 3. ITC Studies on the binding of Bisphosphonates to LmFPPS.

Inhibitor	ΔG (kcal/ mol)	ΔH (kcal/mol)	-TΔS (kcal/mol)	1/Ka (nM)	*LmFPPS K_i (nM)
91B	-10.4	3.15 ± 0.04	-13.6	28.0 ± 9.1	11
46I	-9.5	3.56 ± 0.05	-13.1	119.5 ± 23.4	50
300B	-8.9	4.42 ± 0.07	-13.3	342.5 ± 55.9	9
476A	-9.2	3.16 ± 0.07	-12.4	198.6 ± 57.8	N.D.

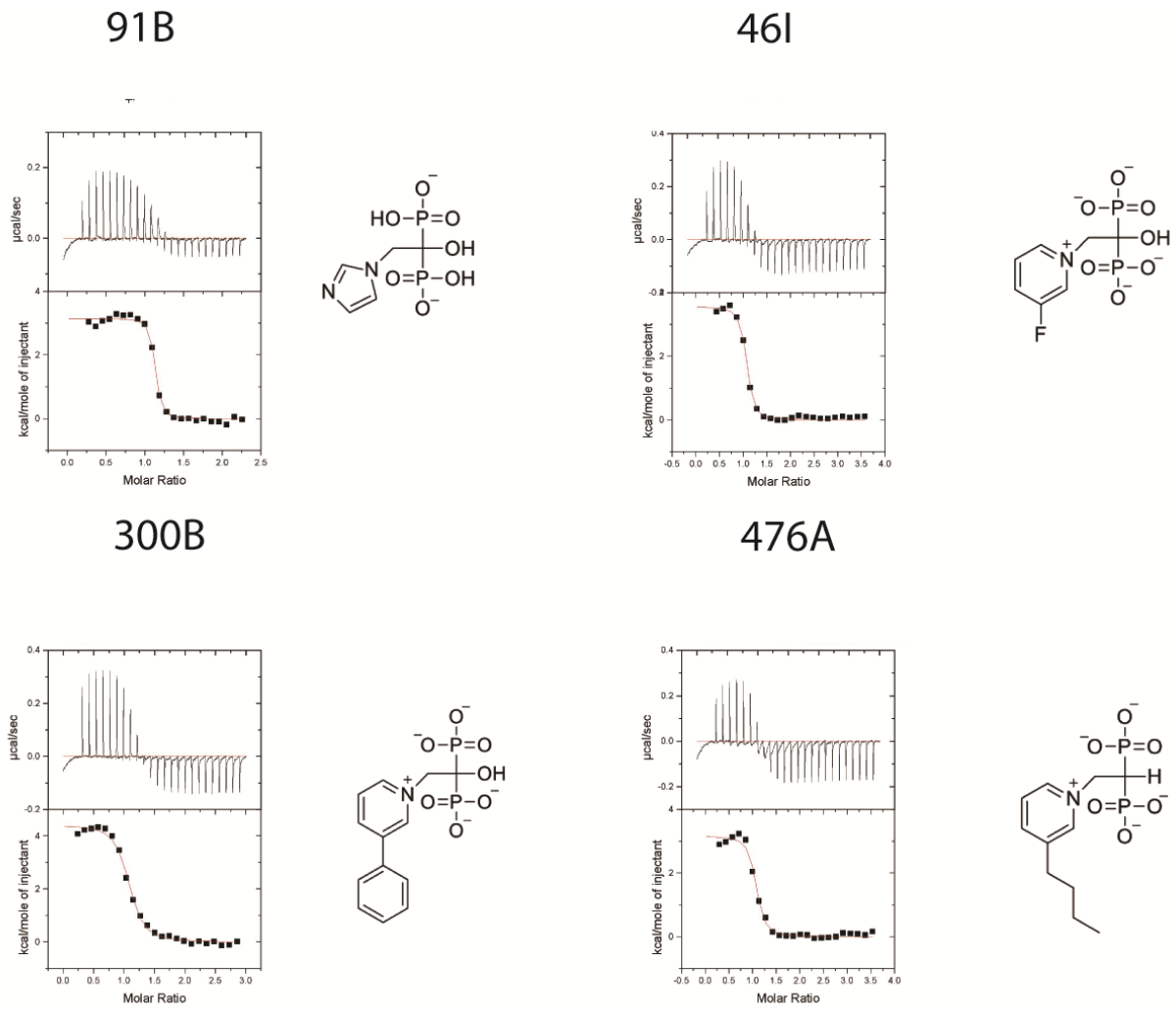

Figure 8. Thermodynamic analysis of LmFPPS binding.

(a, b ,c ,d) Isotherms of inhibitors 91B (a), 46I (b), 300B (c) and 476A (d) to LmFPPS. Top panels display the heat evolved for each injection and the bottom panels shows the integrated heats of injection. The right panel shows chemical formulae. All the curves are fitted to a one-binding site per monomer model.

2.1.9 Mechanistic Insights

Before this work, the coordinates of 55 complexes of FPPSs of diverse species had been deposited in the PDB. None of these had only the homoallylic site occupied, probably indicating that the allylic substrate binds first to the dimer. Reinforcing this hypothesis, the structure of the LmFPPS dimer complex with 46I has the allylic sites occupied while the homoallylic sites are empty. Notably, it is only in the 46I complex that the dimers are not symmetrical: in each dimer, the homoallylic site of one of the monomers is significantly more open than that of the other monomer. The differences are mainly localized in the loop spanning residues 255 to 274 (Fig. 5b, Fig. 9). The open monomers (B and D) provide a clear path for the IPP substrate to reach its binding site. In contrast, the other monomers (A and C) would require changes in their structures in order to allow IPP to reach its binding site. The complex structure of GgFPPS-DMAPP and GgFPPS-GPP (PDB id IUBW and IUBY) in the absence of IPP have a conformation comparable to the 'open' one observed in LmFPPS-46I strengthening the point that this conformation exist and is relevant for the natural substrates. This observation provides structural insight into the ordered binding proposed by Laskovics and Poulter[47]: both allylic sites are occupied first, resulting in an asymmetric structure with one of the monomers in a conformation ideally suited to accept IPP. Binding of IPP to that monomer results in a conformational change that opens the homoallylic site of the other monomer, which closes after binding the second IPP[47]. These changes would result in the symmetric dimer observed in all previous complexes, when both allylic and homoallylic sites occupied.

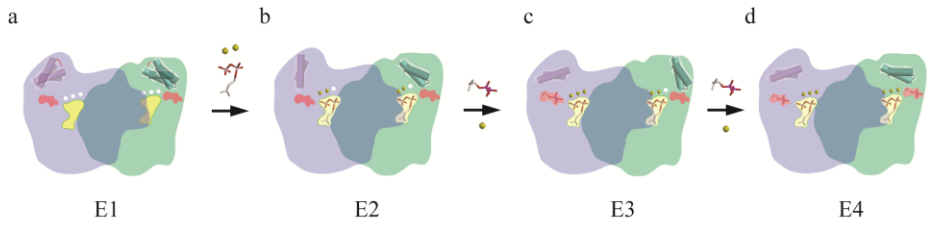

Figure 9. Mechanism of substrate binding to the LmFPPS dimer.

Purple and green shaded regions correspond to the two monomers of the FPPS homodimer. In each monomer, the allylic site is shown as a yellow shaded region and the homoallylic site is in red. Blue spheres represent empty divalent cation sites while the yellow spheres represent the occupied cation sites. The loop 255-274 is shown as either purple or green cylinders. (a) Apo structure (E1) with none of the sites occupied and with the conformation of the loop is either be open or closed. The movement of the loop is indicated by a red curve. (b) Partially open form (E2) in which DMAPP and two divalent cations occupy the allylic sites of each monomer. The loop 255-274 is in a more open conformation in one monomer (purple cylinder) than in the other monomer (green cylinder). This partially open conformation corresponds to that of the LmFPPS-46I-Mg complex. (c) The asymmetry of the conformations of the loop in the two monomers (E3) suggests that IPP and a third divalent cation bind to one of the monomers causing a conformational change priming for the entry of the second IPP molecule. (d) Closed form (E4) as seen in the LmFPPS-300B-IPP-Ca and LmFPPS-476A-IPP-Ca complexes where the allylic, the homoallylic and the 3 divalent cation sites are fully occupied and the residues in the loop 255-274 are in the closed conformation.

2.2 Design, Synthesis, Calorimetry and Crystallographic analysis of 2-Alkylaminoethyl-1,1-Bisphosphonates as inhibitors of *Trypanosoma cruzi* Farnesyl Diphosphate Synthase

Work previously published as:

Design, Synthesis, Calorimetry and Crystallographic analysis of 2-Alkylaminoethyl-1,1-Bisphosphonates as inhibitors of *Trypanosoma cruzi* Farnesyl Diphosphate Synthase.

J Med Chem. 2012 Jul 26;55(14):6445-54.

American trypanosomiasis (Chagas disease) is a major parasitic disease that affects millions of individuals world-wide[64, 65]. *T. cruzi*, the etiologic agent of American trypanosomiasis, has a complex life cycle in which it passes from a blood-sucking Reduviid insect vector to mammals[66]. It multiplies in the insect gut as an epimastigote form and is spread as a non-dividing metacyclic trypomastigote from the insect feces by contamination of intact mucosa or of wounds produced by the blood-sucking activity of the vector. In the mammalian host, the parasite proliferates intracellularly in the amastigote form and is subsequently released into the blood stream as a non-dividing trypomastigote.[66] In humans, spread of Chagas disease can also take place *via* the placenta or by blood transfusion.[67, 68] The occurrence of American trypanosomiasis in countries where the disease is not endemic has been attributed to the second mechanism.[67, 68] Chemotherapy for this neglected disease, based on old and empirically discovered drugs, is not very effective.[69] Thus, it is critical that we develop new safe drugs based on knowledge of the biochemistry and physiology of the microorganism. 2-alkylaminoethyl-1,1-bisphosphonates have emerged as a new avenue for the development of compounds active against Chagas disease.

Bisphosphonates of general formula **1** (Fig. 10) are metabolically stable pyrophosphate (**2**) analogues in which a methylene group replaces the oxygen atom bridge between the two phosphorus atoms of the pyrophosphate moiety. Substitution at the carbon atom with different side chains has generated a large family of compounds.[70-73] Bisphosphonates became compounds of pharmacological importance since calcification studies were done more than 40 years ago.[74-76] Currently, several

bisphosphonates (Fig. 10) such as pamidronate (**3**), alendronate (**4**), risedronate (**5**), and ibandronate (**6**) are in clinical use for the treatment and prevention of osteoclast-mediated bone resorption associated with osteoporosis, Paget's disease, hypercalcemia, tumor bone metastases, and other bone diseases.

Selective action on bone is based on binding of the bisphosphonate moiety to bone mineral.[43] It has been postulated that the parasite's acidocalcisomes, organelles equivalent in composition to the bone mineral, may accumulate bisphosphonates and facilitate their antiparasitic action.[43] In the case of bone, bisphosphonates act by a mechanism that leads to osteoclast apoptosis.[77] The site of action of aminobisphosphonates has been narrowed down to the isoprenoid pathway and, more specifically, to inhibition of protein prenylation.[78] Within the isoprenoid pathway, farnesyl pyrophosphate synthase (FPPS; also called farnesyl diphosphate synthase) was identified as the main target of bisphosphonates.[55, 58, 79-82] FPPS catalyses two consecutive 1´-4 condensation reactions between an allylic (DMAPP or GPP) and a homoallylic substrate (IPP) to give a final product FPP. These reactions constitute the two committed steps in the biosynthesis of farnesyl pyrophosphate. In the first step it catalyzes the 1´-4 condensation of one molecule of IPP (homoallylic substrate) and one molecule of DMAPP (allylic substrate) to give GPP. In the second step it condenses one molecule of GPP and one molecule of IPP. Inhibition of the enzymatic activity of FPPS blocks farnesyl pyrophosphate and geranylgeranyl pyrophosphate formation, compounds which are required for the post-translational prenylation within osteoclasts of small GTPases such as Rab, Rho and Rac.[83]

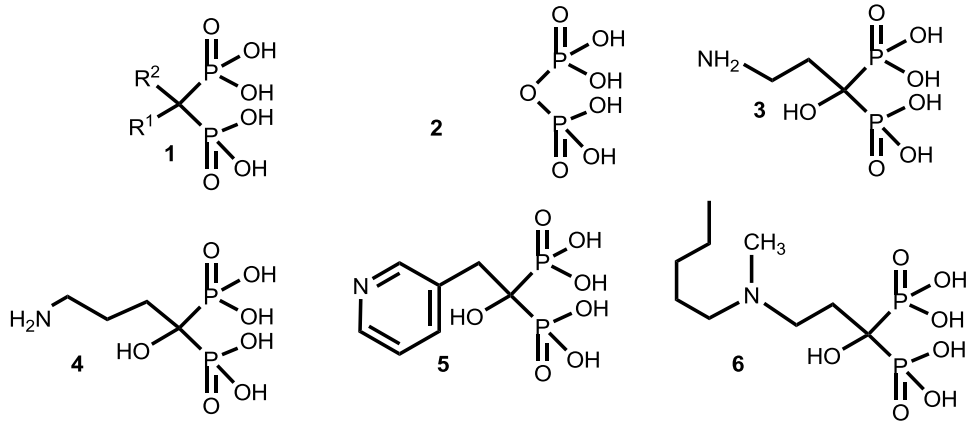

Figure 10. General formulas and chemical structures of pyrophosphate and bisphosphonates.

1-general bisphosphonate; 2-pyrophosphate; 3-6-representative FDA-approved bisphosphonates clinically employed for different bone disorders: 3, palmidronate; 4, alendronate; 5, residronate; 6, ibandronate.

Besides their effectiveness in long-term treatment of bone disorders, bisphosphonates exhibit a wide range of biological activities that include, in addition to stimulation of γδ T cells of the immune system,[84] antibacterial,[85] herbicidal,[86] antitumor[87-90] and antiparasitic activities.[35, 39, 91-93]

In vivo assays showed that risedronate can significantly increase survival of *T. cruzi*-infected mice[42]. Besides being effective growth inhibitors of *T. cruzi* in *in vitro* and *in vivo* assays without toxicity to the host cells[43], bisphosphonates were found to be also effective against pathogenic trypanosomatids other than *T. cruzi*. Those include *T. brucei rhodesiense*, *Leishmania donovani*, and *L. mexicana* as well as apicomplexan parasites such as *Toxoplasma gondii* and *Plasmodium falciparum*.[40, 92-99] These results point to bisphosphonates as potential candidates for chemotherapy of a range of neglected infectious diseases. They have the advantage, among other favorable characteristics, that they are relatively inexpensive and easy to synthesize. Furthermore,

one may assume a low toxicity for bisphosphonate-containing drugs considering that many bisphosphonates are FDA-approved drugs that have been widely used for many years in the long-term treatment of bone disorders.

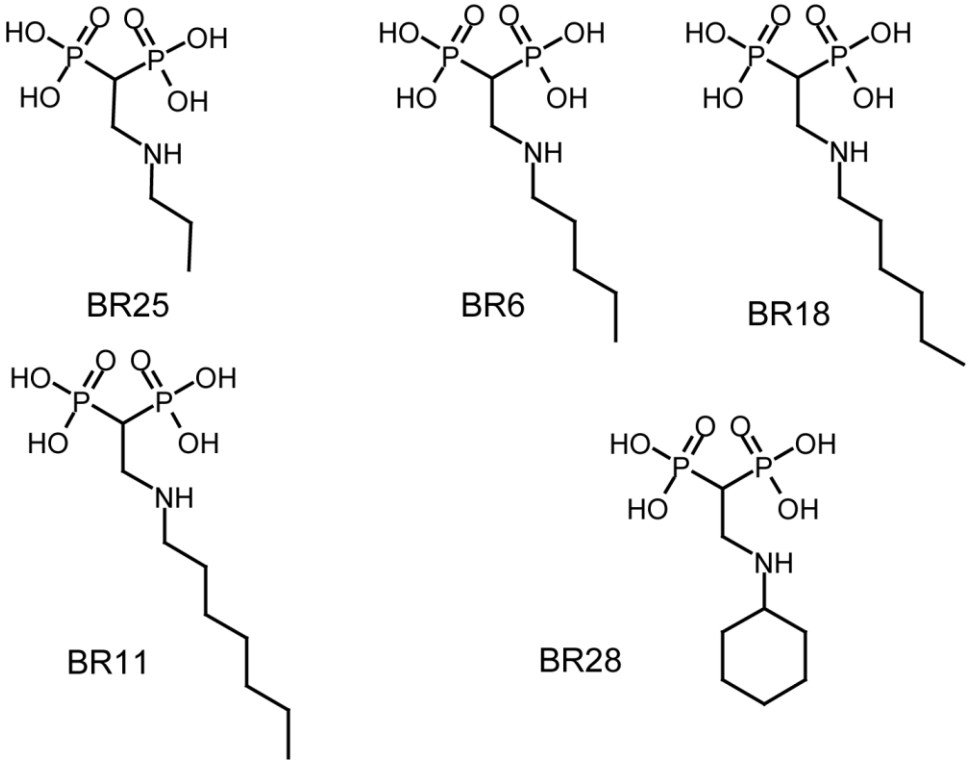

Figure 11. Bisphosphonate drugs used in this study.

[2-(n-propylamino)ethane-1,1-diyl]bisphosphonic acid (BR25 = **10**); [2-(n-pentylamino)ethane-1,1-diyl]bisphosphonic acid (BR6 = **11**); [2-(n-hexylamino)ethane-1,1-diyl]bisphosphonic acid (BR18 = **12**); [2-(n-heptylamino)ethane-1,1-diyl]bisphosphonic acid (BR11 = **13[95, 97, 99]**); [2-(cyclohexylamino)ethane-1,1-diyl]bisphosphonic acid (BR28 = **14**).

We studied both structural and thermodynamic interactions of five 2-alkylaminoethyl-1,1-bisphosphonates with *T. cruzi* FPPS (TcFPPS; Fig. 11). The structures show that the inhibitors bind to the allylic site of the enzyme with the phosphates of the bisphosphonates coordinating three Mg^{2+} ions that bridge the compound to the enzyme in a manner similar to that observed for the physiological substrates[45, 47, 100]. The alkyl chains of the inhibitors bind within a long cavity

normally occupied by the isoprenoid chain of the allylic substrate (Fig. 12). The inhibitors bind to TcFPPS with high affinity despite having unfavorable enthalpy of binding. The favorable entropy that results from burying the hydrophobic alkyl chain is the main binding driving force.

Although several bisphosphonate families have been shown to inhibit the trypanosomal FPPS, the lack of pharmacokinetic studies on these compounds suggests that it is still important to expand the number of compounds in the pipeline, especially with compounds of high affinity.

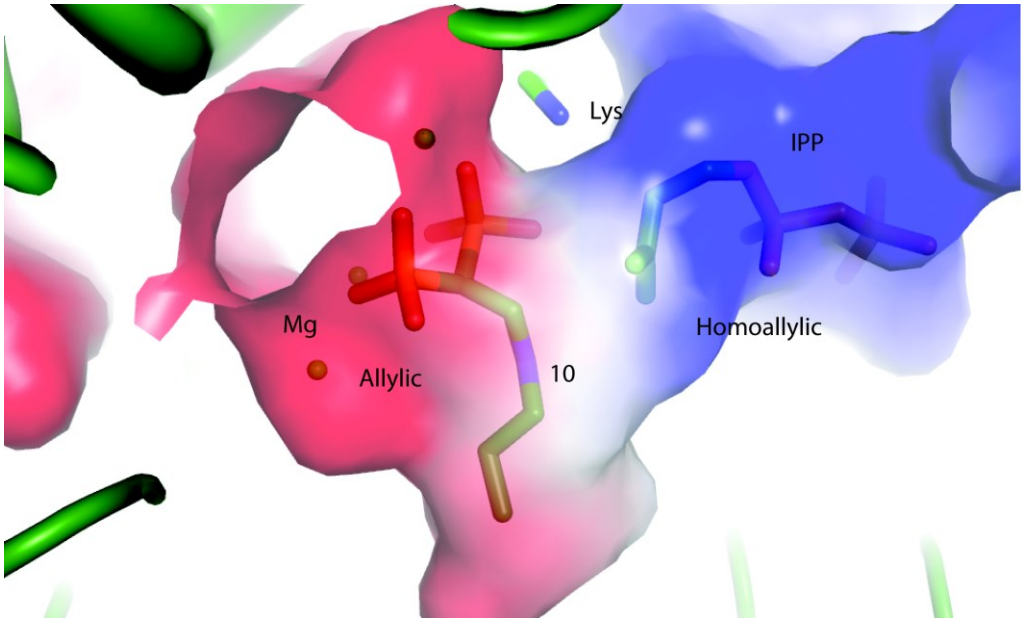

Figure 12. Electrostatic map of Allylic and Homoallylic site in TcFPPS.

The allylic site is the part of the active site occupied by Mg and the bisphosphonate **10**. The Homoallylic site is occupied by IPP. Magnesiums are shown in CPK model while the ligands **10** (BR25) and IPP are shown as a stick model. The surface shows positive potential as blue and negative as red.

The structural and thermodynamic information presented here provides the basis for the design of novel, more effective compounds for the treatment of Chagas disease. In particular, new inhibitors with strategically placed double bonds and methyl-group branches are predicted to have significantly increased affinity.

2.2.1 Structure of the inhibitor complexes

Like the FPPS from other species, including humans, [58, 101] the farnesyl diphosphate synthase of *T. cruzi* (TcFPPS) is a physiological homodimer (monomers A and B). The structures of TcFPPS in complex with five bisphosphonates BR25, BR6, BR18, BR11 and BR28 (resolutions between 2.01 Å and 3.0 Å; Table 1) each contained, in addition, 3 divalent cations (Mg^{2+}) and isopentenyl pyrophosphate (IPP) or SO_4^{-2} (BR11-TcFPPS complex has SO_4^{-2}). Crystals of the complexes belong to space group $P6_122$; four of the complexes have an average cell dimension of 392 Å along c-axis, 5 Å shorter than the equivalent dimension in the apo structure[7] (Table 3) indicating that the structures of the complexes pack more compactly than that of the apo enzyme.

Table 4. Structures of TcFPPS complexes: Data collection and Refinement Statistics.

Crystal	TcFPPS+ IPP+ BR6 + Mg^{2+}	TcFPPS+ IPP+ BR11+ Mg^{2+}	TcFPPS + IPP+ BR18+ Mg^{2+}	TcFPPS+ IPP+ BR28+ Mg^{2+}	TcFPPS+ IPP+ BR25+ Mg^{2+}
Space group	$P6_122$				
Cell dimensions(Å)	a = 57.9; b = 57.9; c = 392.4				a = 103.2 b = 103.2 c = 386.6
X-ray Source	BNL-X6a	BNL-X6a	BNL-X6a	BNL-X6a	BNL-X6a
Res(Å)	50.0-2.1	50.0-2.01	50.0-2.65	50.0-3.05	50.0-2.35
Unique Reflections	22,705	27,252	12,287	7,407	49,874
I/σ	23.6(4.3)	34.3(6.2)	38.0(7.8)	46.9(16.8)	26.6(2.2)
Completeness (%)	93.2 (98.2)	97.8(98.7)	95.7(99.8)	87.8(90.3)	96.0(93.7)
R_{merge} (%)	11.3(50.9)	8.0(34.6)	10.5(47.3)	6.9(14.3)	9.0(52.0)
	Refinement				
R_{cryst} (%)	22.1	20.3	23.6	23.1	22.0
R_{free}	28.4	26.7	30.7	29.6	28.5
Monomer in ASU	1	1	1	1	3
Total Atoms	3,037	3,205	2,960	2,916	9,014
Protein atoms	2,900	2,900	2902	2854	8701
Water molecules	89	256	23	3	161
	R.m.s deviations				
Bond length (Å)	0.021	0.02	0.008	0.007	0.009
Angle (°)	1.82	1.83	1.13	0.97	1.21
	B-factor($Å^2$)				
Protein	31.14	28.33	51.53	46.81	33.36
Allylic	36.23	27.25	40.18	47.54	29.54
Homoallylic	58.19	59.30	51.17	49.13*	44.72
H_20	35.01	35.59	34.12	26.10	30.51

*Occupancy : 0.6

The structures were determined by direct refinement or by molecular replacement (complex BR25-TcFPPS) using the structure of the *Trypanosoma cruzi* FPPS in complex with alendronate and IPP (1YHM). After initial refinement, 2Fo-Fc maps showed excellent density for the bound inhibitors in the region corresponding to the allylic site. In the homoallylic site, electron density for IPP is seen in four structures – BR25, BR6, BR18 and BR28; in BR11 a SO_4^{-2} ion occupies the homoallylic site.

In all cases, three Mg^{2+} ions bridge the phosphates of the inhibitors to the protein. The conserved aspartate residues of the two-aspartate rich motifs DDXXD (first aspartate rich motif: FARM, residues 98-102; second aspartate rich motif: SARM, residues 250-254) bind three divalent cations (Mg^{2+}) that are in turn coordinated by the phosphate backbone of the bisphosphonates (Fig. 13a; BR6). The IPP is bound to the enzyme by interacting directly with arginine residues (Arg51, Arg108, and Arg360 (Fig. 13b). The conserved RRG sequence (residues 107-109) of the loop following the FARM region and residues GK (263 and 264) in the loop following the SARM region are in the conformations usually seen in the closed form of the enzyme with both the allylic and homoallylic sites occupied. In all five structures the bisphosphonate, occupies the allylic site, and interacts with 3 divalent Mg^{2+} ions. Ligand waters complete the octahedral coordination of the ions.

Structural alignment of the four complexes with *n*-alkyl chains shows that the phosphate backbones of the bisphosphonates interact with the same residues of the protein, located near the top of the active site (Fig. 13c; Fig. 14a). However, deeper into the active site there are a small number of significant differences (Fig. 14b). In the BR18

and BR11 complexes, Tyr94 and Gln167 both move to accommodate the bisphosphonates with the longer alkyl chains. In the complex with BR11, the bisphosphonate with the longest alkyl chain, the end of the inhibitor bound to monomer A is at a distance of 3.5 Å from Ile 129 from monomer B. This additional favorable van der Waals interaction contributes to the tighter binding of BR11 (Table 5) in comparison to the slightly shorter BR18 (one fewer carbon).

It was proposed in earlier studies that His93 and Tyr94 (TcFPPS numbering) form the "floor" of the allylic site and determine the maximum length of the allylic substrates that can bind to the enzyme[102] and by extension the length of the inhibitors. The complexes BR11-TcFPPS and BR18-TcFPPS show that Tyr94 adopts a different conformation to accommodate longer alkyl chains (Fig. 14b). Earlier studies with avian FPPS revealed that when Phe112 and Phe113 (equivalent to His93 and Tyr94 of TcFPPS) were replaced by residues with smaller side chains (Ala and Ser respectively), the mutated enzyme produced geranyl geranyl diphosphate (20 carbons)[57]. Also, in some species, geranyl geranyl diphosphate synthases contain smaller amino acids such as serine or threonine in the position equivalent to TcFPPS Tyr94 indicating that Tyr94 may be important in determining final product length[61]. These observations point to His93 and Tyr94 of chain A and Ile129 of the B chain as the residues that determine maximum permissible alkyl chain length.

2.2.2 Comparison of the BR28-TcFPPS and BR25-TcFPPS complexes

In the BR28-TcFPPS structure, the cyclohexyl moiety adopts a chair conformation. Structural alignment of the BR28-TcFPPS and BR25-TcFPPS complexes shows that packing of BR28 to the enzyme is not as tight as that of BR25. Also, residue Gln167, one of the conserved residues in α-helix F, adopts a different conformation in the two complexes (Fig. 13d.). The same is true about another conserved residue, Tyr211: in BR28 its hydroxyl points away from bisphosphonate moiety. Interestingly, in the BR28 complex Tyr211 points towards the isoprenyl chain of the bound IPP and, as a result, it affects the IPP conformation.

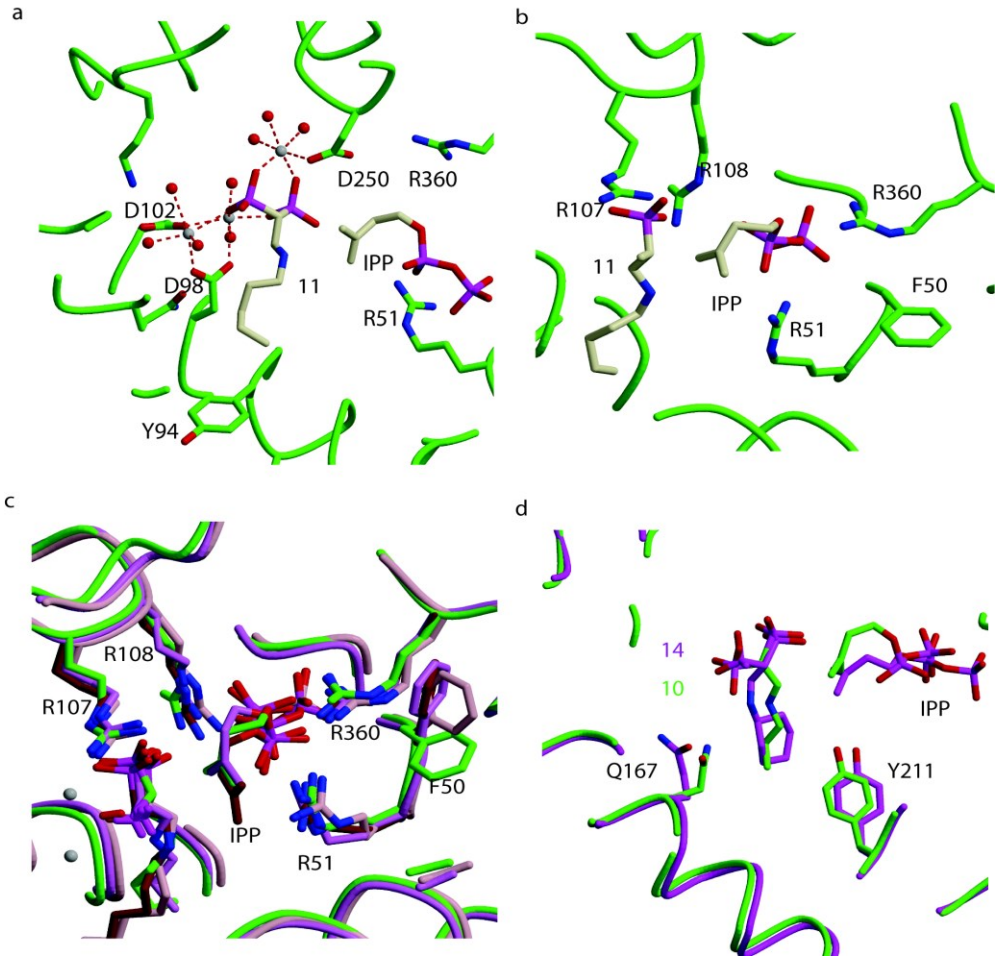

Figure 13. Binding of bisphosphonates in various complexes of TcFPPS.

(a) TcFPPS in complex with **11**(BR6), IPP and 3 divalent cations. Water molecules are shown as red spheres and Mg^{2+} in white. Protein backbone and residues of the active site are shown in green color. **11**(BR6) and IPP are shown in cream color. Residues from the FARM and SARM are shown coordinating with Mg^{2+} ions. The basic amino acids Arg360 and Arg51 are observed to interact with the diphosphate moiety of IPP. (b) Homoallylic site of TcFPPS in complex with **11**(BR6) (cream) and IPP (cream). IPP interacts with the basic amino acids Arg51 and Arg360. Arg107 and Arg108, from the loop after first aspartate rich region, interact with the inhibitor in the allylic site (**11;**BR6). (c) Structural overlap of the four BPs with *n*-alkyl chains (**10-13**) in complex with TcFPPS + Mg^{2+} + IPP (green). (d) Structural overlap of TcFPPS in complex with **10** (BR25) (green) and with **14** (BR28; magenta). Residues in the TcFPPS-BR25 complex are shown in green color and those of TcFPPS-BR28 complex in magenta. Key differences in the conserved interactions of the ligands with residues of the active site are shown.

2.2.3 Inhibitor Affinities

Bisphosphonates derived from fatty acids have become interesting potential antiparasitic agents, especially 2-alkylaminoethyl derivatives, which were shown to be potent growth inhibitors of the most clinically relevant form of *T. cruzi* with IC_{50} values in the nanomolar range against the target enzyme[95, 98]. Compounds BR6−BR28 are representative members of the 2-alkylaminoethyl family of bisphosphonates, which have proven to be far more efficient growth inhibitors of trypanosomatids than their parent drugs 1-hydroxy-, 1-alkyl-, and 1-amino-bisphosphonates such as compounds **7**, **8** and **9** (Fig. 15).[96, 98, 99] Compounds BR6−BR28 inhibit the enzymatic activity of *Tc*FPPS with IC_{50} values of 38 nM, 1.84 □M, 0.49 □M, 58 nM, 13 nM, respectively (Table 5).[97]

2.2.4 Thermodynamic Data

The interactions of *Tc*FPPS with 2-alkylaminoethyl bisphosphonates BR6, BR25, BR11 and BR18 were studied by isothermal titration calorimetry at 28 °C. (ITC data for *reversible* binding of BR28 to TcFPPS could not be obtained.) The four compounds with *n*-alkyl chains, bind to the target enzyme with a positive, unfavorable enthalpy change (Fig. 16; Table 5), in agreement with previous studies with other bisphosphonates[6]. This unfavorable enthalpy is compensated by large favorable entropy that is itself determined by the difference between to opposite effects. As the inhibitor molecules bind, the single bond rotations around the C—C bonds of the alkyl chain become frozen in the complex resulting in a loss of conformational entropy that becomes larger as the number of carbons in the alkyl chain increases. At the same time, the favorable entropy from the

burial of the hydrophobic alkyl chain also increases with chain length, resulting in a very fine balance between these two effects. The values of the unfavorable binding enthalpy also vary significantly among the inhibitors. BR18 is the most unfavorable by 1.5-2.0 Kcal/mol.

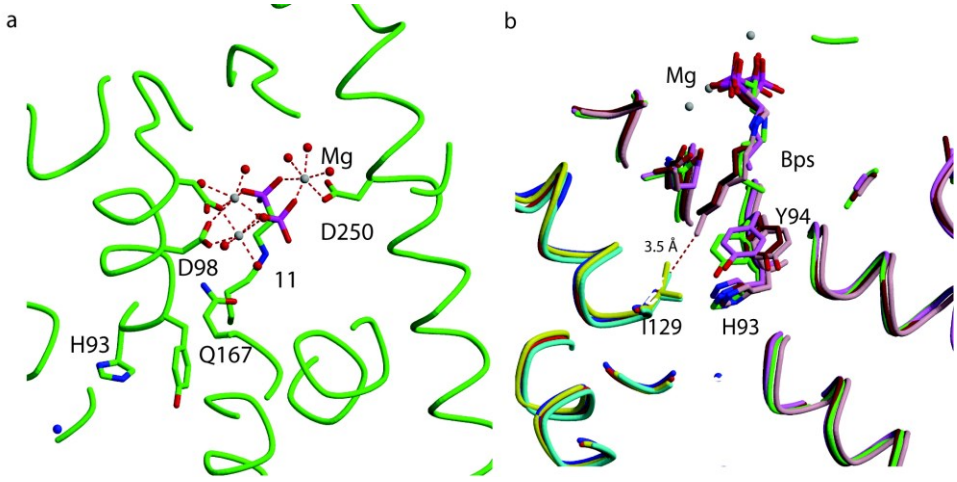

Figure 14. Allylic site binding of inhibitors in various TcFPPS-Bps complexes.

(a) TcFPPS in complex with **11 (BR6)** and 3 divalent cations. Water molecules are shown as red spheres, Mg^{2+} in white. The TcFPPS protein backbone and some residues in the active site are shown in green color. **11** is shown as a stick model in green color. Residues from the first and second aspartate rich regions are shown coordinating the Mg^{2+} ions. (b) Structural overlap of TcFPPS in complex with four *n*-alkyl chain bisphosphonates BR6, BR25, BR11 and BR18. Residues His93, Tyr94, Ile129 (monomer B) at the "bottom" of the allylic site are shown. Monomer A of the TcFPPS-BR6 complex is shown in green, the TcFPPS-BR11 complex in pink, TcFPPS-BR18 complex in brown, TcFPPS-BR25 complex in violet while monomer B is shown in red, cyan, yellow and blue respectively. The distance between the terminal carbon of the longest bisphosphonate BR11 and Ile 129 of monomer B is 3.5 Å.

The high affinity of BR28 (IC_{50} 13 nM) can be rationalized based on the same arguments. TcFPPS binds BR28 in a manner similar to BR25, suggesting that it would have a similar enthalpy of binding (not measured), although somewhat more unfavorable due to changes in the conformations of Gln167 and Tyr211 described above. However, BR28 buries a large hydrophobic surface without the loss of conformational entropy of the *n*-alkyl chain

experienced by the other inhibitors: the conformational flexibility of the ring is highly restricted even in the unbound state.

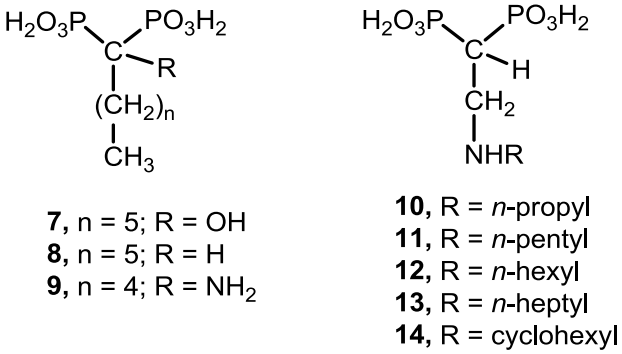

Figure 15. Chemical structures of representative bisphosphonic acids derivatives.

Furthermore, binding in the more stable chair conformation not only reduces the loss of entropy but also avoids the enthalpic penalty of binding the less favorable boat conformation.

The inhibition data (IC_{50}) of bisphosphonates BR6, BR25, BR11 and BR18 against TcFPPS are in excellent agreement with the K_d's obtained in the ITC experiments (Table 5). These results and the structural data taken together indicate that inhibition results from binding of these inhibitors to the allylic portion of the catalytic site of the enzyme. It is likely that other closely related bisphosphonates that effectively inhibit the enzymatic activity of TcFPPS also do so by binding to the allylic site.[98] The data for BR11 can also be fit using two different sites per dimer (see Fig. 16 and Table 5 and their footnotes). This is similar to previous data on other nitrogen-containing bisphosphonates[6]. One reason for this behavior of BR11 may be its size. Like some of

the other large bisphosphonates, binding of BR11 to one site of the dimer, modifies the affinity of the other monomer.

2.2.5 Towards the design of new bisphosphonate TcFPPS inhibitors

As mentioned above, binding of these inhibitors is enthalpically unfavorable. The favorable entropy, which dominates the favorable free-energy, results from a delicate balance two opposing effects: the unfavorable loss of conformational entropy, due to freezing of single bond rotations of the inhibitor (and binding site side chains), and the favorable increase of entropy associated with burial of the hydrophobic alkyl chains. With the shortest compound, *n*-propyl, the balance produces the tightest binding of the

Table 5. ITC Studies on the binding of bisphosphonates to TcFPPS.

Lig	Carbons in *n*-alkyl	ΔG (kcal/ mol)	ΔH (kcal/mol)	ΔS (cal/m ol/K)	1/Ka (nM)	IC^{*}_{50} (nM)
BR25	3	-10.43	6.35 ± 0.07	56.1	25.0 ± 6.3	38.0
BR6	5	-8.15	5.22 ± 0.11	44.7	1030 ±170	1840
BR18	6	-8.72	7.87 ± 0.11	55.4	400 ± 63	490
BR11	7	-9.88	5.65 ± 0.09	51.9	58.8 ± 20.4	58.0
			†(6.39 ± 0.36; 4.62 ± 0.44)		†(10.2 ± 7.3; 38.3 ± 11.2)	

*IC50 were calculated before[97] †Values calculated using 2-site model.

Comparison of the structure of the BR11-TcFPPS complex with the previously determined structure of the chicken FPPS (GgFPPS) in complex with GPP (geranyl pyrophosphate) provides crucial information for guiding the design of improved inhibitors: the N1 of BR11 occupies the same position in the binding site as the C1 of the isoprenyl chain GPP (Fig. 17) and the rest of the chains align up to the C6 of BR11 that overlaps with C7 of the GPP. C7 of GPP is a tertiary carbon with two methyl groups while the equivalent carbon of BR11 (C6) has only one methyl. The terminal methyl of BR11 occupies a position series. Increasing the length of the alkyl chain to pentyl or hexyl reduces the affinity by over an order of magnitude. This change seems to imply that by the addition of two or three methylenes, the increase in the loss of conformational entropy is greater than the additional entropy gain due to burial of the longer chain (more so for the pentyl than for the hexyl). This tendency is reversed when the *n*-alkyl chain is seven carbons long (BR11 vs. BR18, Table 5). This observation suggests that increasing the alkyl chain further could generate compounds with higher affinity. However, analysis of the structure of the complex of TcFPPS with the *n*-heptyl inhibitor shows that increasing the *n*-alkyl chain past seven carbons would result in clashes with residues of the enzyme: in any of its possible positions the eighth carbon would clash with either Tyr94, His93, or Ile129 of chain B.

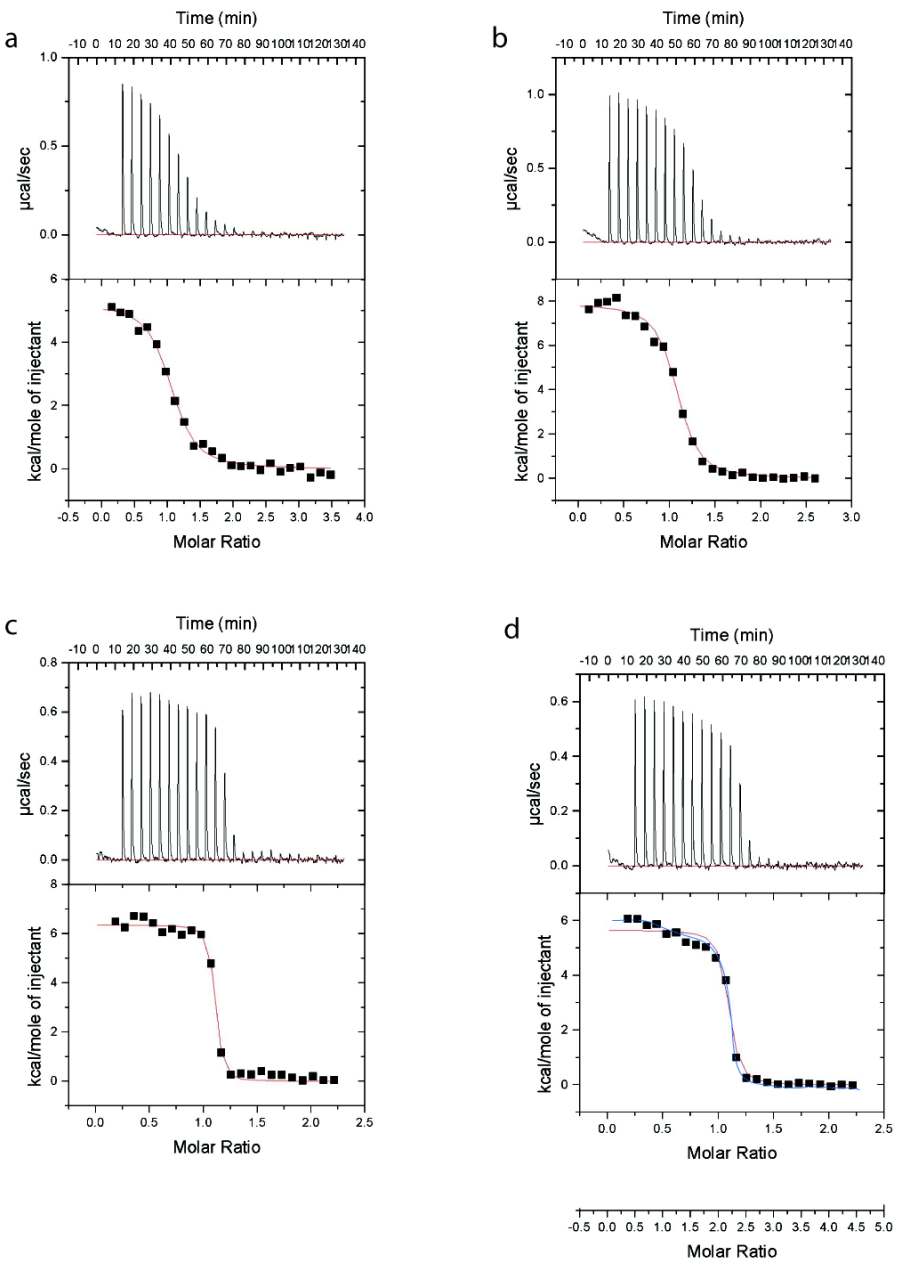

Figure 16. ITC studies of N-Bps and TcFPPS binding.

(a) BR6. (b) BR18. (c) BR25. (d) BR11. BR11 can be fit either as two identical sites (one per monomer; red) or as two different sites (two per dimer; blue).

between the positions occupied by the two GPP methyls, rendering this portion of BR11 less complementary to the binding site. Adding a methyl group to the C6 of BR11 is likely to result in a better inhibitor. The same is true of the C3 methyl of GPP: adding a methyl group at the C2 of BR11 can fill this pocket. Furthermore, the bound conformation of BR11 is compatible with the double bonds of GPP, suggesting that introducing double bonds at C1 and C5 of BR11 will freeze the compound in the bound conformation. This modification would reduce the loss of conformational entropy without affecting the binding enthalpy. The resulting compound with a 2,6-dimethyl-1,5-diene would be an excellent mimic of the bound GPP; however it would contain a labile enamine functionality that renders the compound too unstable to be considered a useful inhibitor. These observations point to a 2-alkylaminoethyl-1,1-bisphosphonate with an (*E*)-2-2,6-dimethylhepta-2,5-diene chain (compound **21**, Fig. 18) as a highly promising lead compound for the next generation of bisphosphonate TcFPPS inhibitors (Fig. 17b; Fig. 18). Molecular modeling using MOE (Molecular Operating Environment, Chemical computing group; Quebec, Canada) showed that the 2,5 diene chain can bind the enzyme in a conformation that still mimics that of the bound geranyl diphosphate. It appears that the affinity of BR25 can also be improved by an equivalent modification. Replacement of the propyl chain by an isobutyl-2-ene (compound **20**, Fig. 18) would result in a compound that binds the enzyme mimicking DMAPP. In addition, the compounds equivalent to **20** and **21** but lacking the double bond at the 2- positions may also show high affinity for the enzyme.

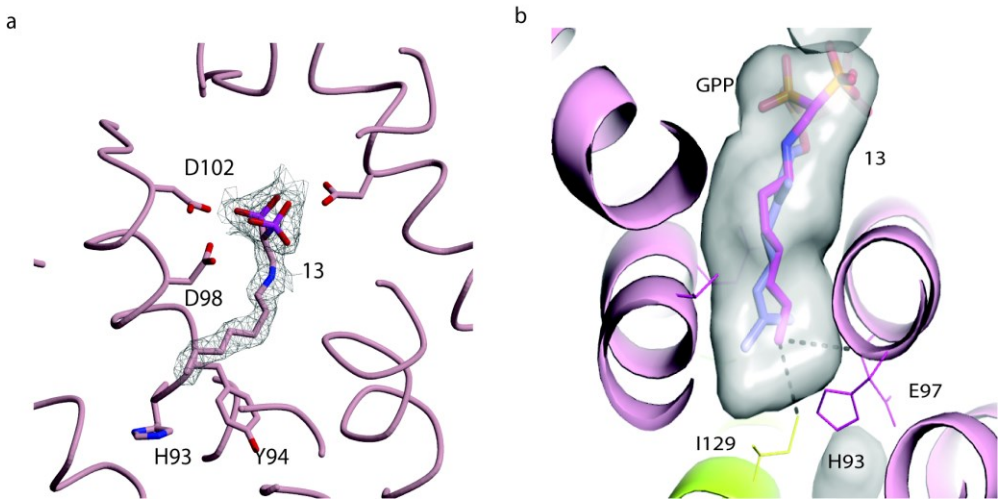

Figure 17. Overlap of GPP and BR11 (**13**)

a) Allylic site of BR11-TcFPPS complex. BR11, amino acids are shown in stick representation (pink). Portion of the $2mF_o$-DF_c electron density corresponding to the inhibitor BR11 is shown in grey color. b) Structural overlap of BR11-TcFPPS complex with the chicken FPPS-GPP complex (PDB: 1UBW). TcFPPS is shown in ribbon model (green). The ligands BR11 (pink) and GPP (blue) in stick representation. The chicken FPPS is not shown in the figure, only it's GPP.

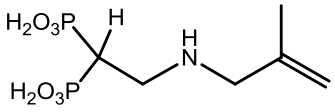

20

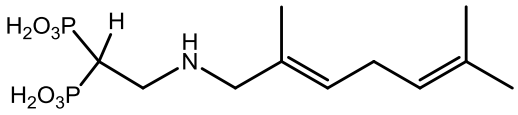

21

Figure 18. New proposed bisphosphonates.

3. Methods

3.1 Experimental Procedures: LmFPPS project

3.1.1 Cloning, Expression And Purification

LmFPPS was cloned and expressed as reported previously[103]. Briefly, DNA coding for LmFPPS (with an N-terminal His-Tag and a thrombin cleavage site) was cloned into a pET28a vector (Novagen). BL21(DE3) *E. coli* cells transformed with this plasmid were grown in LB medium until they reached an OD_{600} of 0.8 and were then induced with 0.1 mM IPTG at 37 ^{o}C. Cells were harvested 3h after induction and were washed in buffer A (50 mM NaH_2PO_4 pH 8.0 300 mM NaCl, 10 mM imidazole, 1 mM TCEP). After the cells were broken with a micro-fluidizer, the lysate was centrifuged for 30 minutes at 12000 rpm, and the supernatant loaded onto a HisTrap Ni^{2+} chelate affinity column equilibrated with buffer A. Protein was eluted using a linear gradient of 0-100% of buffer B (50 mM NaH_2PO_4 pH 8.0 300 mM NaCl, 500 mM imidazole, 1 mM TCEP). The poly-histidine tag was cleaved by digestion with thrombin, and the sample loaded onto an anion exchange column (binding buffer: 20 mM Tris pH 8.2, 50 mM NaCl, 1 mM TCEP) and eluted with 20 mM Tris pH 8.2, 1 M NaCl, 1 mM TCEP. The eluate was further purified through a second round of nickel affinity chromatography, collecting the flow through. The protein was dialyzed against 20 mM Tris pH 8.2, 150 mM NaCl, 1 mM TCEP and concentrated to 15 mg/mL.

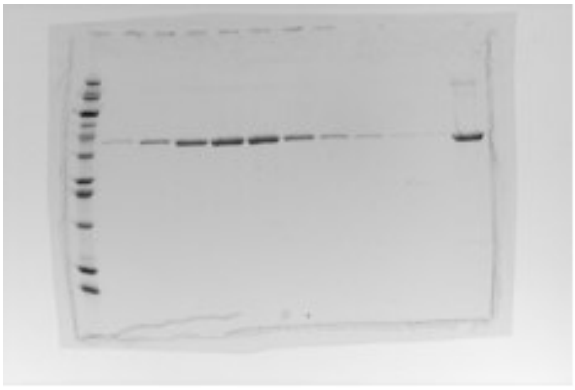

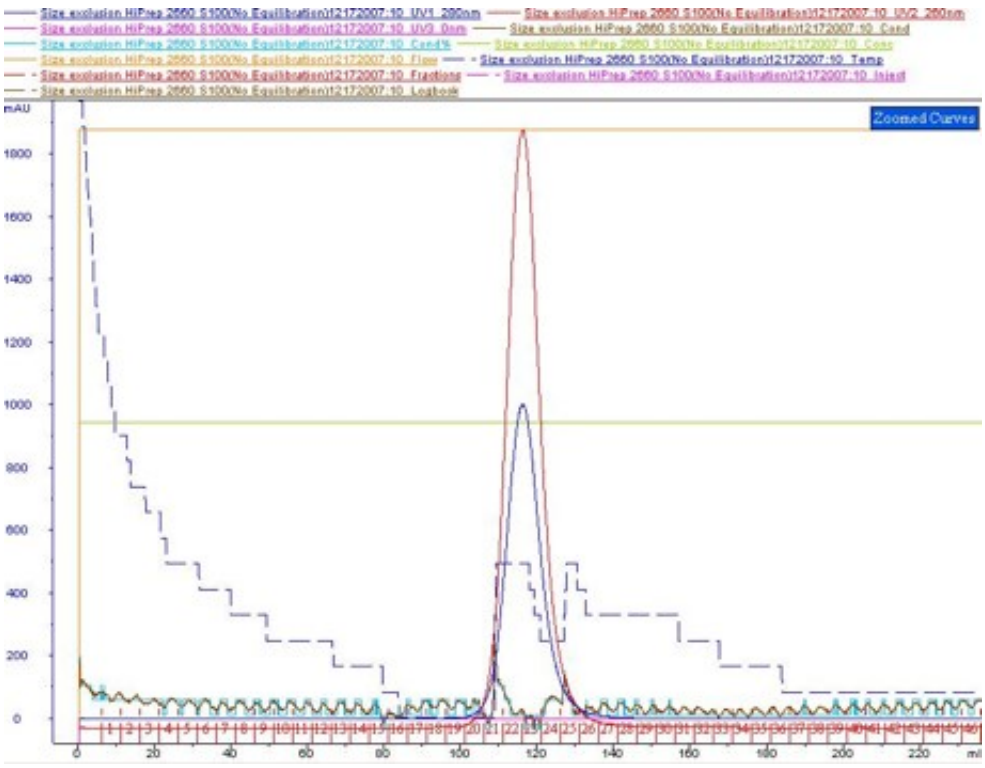

Figure 19. SDS page gel and size exclusion chromatography.

3.1.2 Crystallization

After identifying crystallization conditions using an incomplete factorial set with 600 nL hanging drops[104], crystals for use in data collection were grown by vapor diffusion using a 1:1 ratio of the protein and reservoir solutions (15-25 % PEG 3350, 0.1-0.2 M calcium acetate and 0.1 M MES sodium salt, pH 6.5). The protein complex solution used for co-crystallization contained LmFPPS at 12.5 mg/ml, 250 μM of the inhibitor, 250 μM IPP and 1 mM $MgCl_2$. Crystals belonging to the orthorhombic space group $P2_12_12_1$ appeared within 1-2 days (Fig. 20). Crystals of 300B and 476A had the same cell dimensions, but the cell of the 46I complex was significantly larger (Table 1.).

3.1.3 Data Collection

Crystals, cryo-protected in mother liquor, were flash frozen at 100 K. Diffraction data for the 300B and 476A complexes were collected in-house using an FRE X-ray source with an Raxis IV detector, and for the LmFPPS-46I-Mg complex at beam line 31A of the Advanced Photon Source (APS). Data were processed and scaled with the HKL 2000 suite[105] (Table 1, Fig. 21).

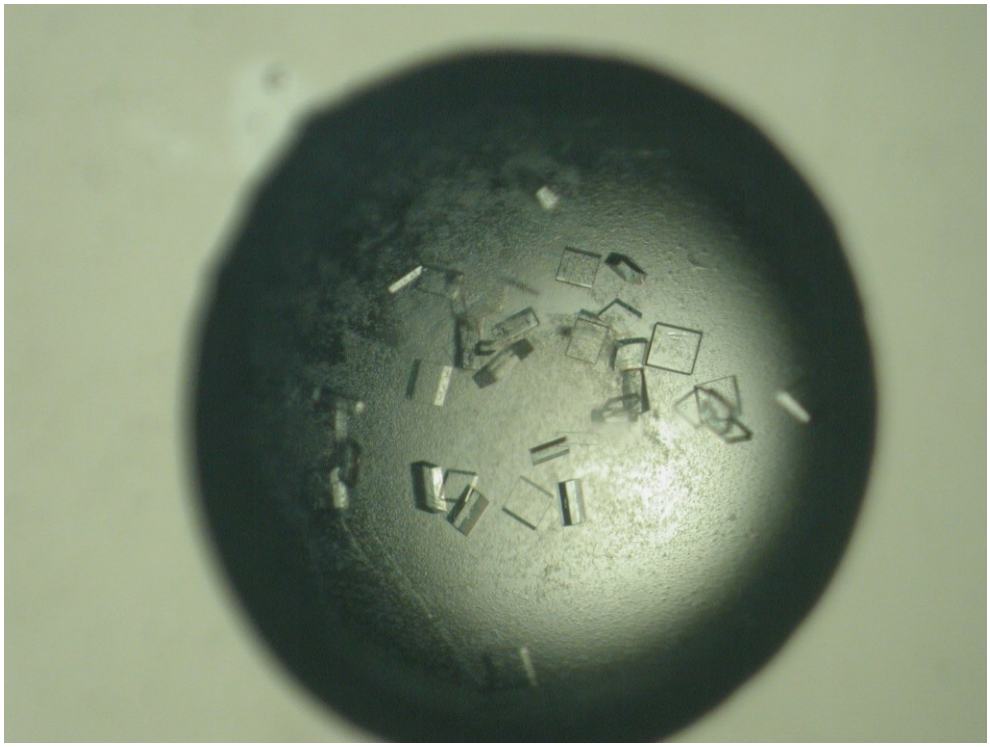

Figure 20. Crystals of 476A-LmFPPS complex.

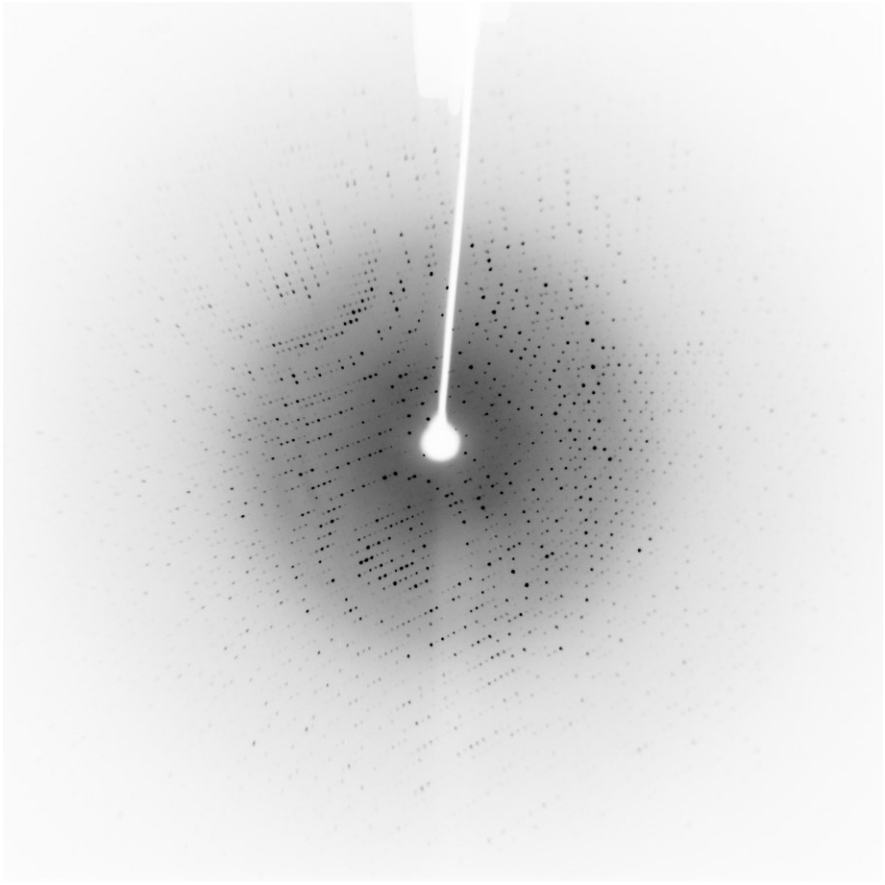

Figure 21. X-ray diffraction pattern of the LmFPPS-476A complex.

3.1.4 Structure Determination and Refinement

The LmFPPS structure was determined by molecular replacement with the program Amore[106] using the coordinates of the FPPS from *Trypanosoma cruzi* (1YHK; 60% sequence identity[7]) as the search model. After changing the sequence to that of the LmFPPS with the program O[107], iterative cycles of refinement and rebuilding were carried out with REFMAC5[108-110] and COOT[111]. Progress of the refinement was monitored by following the R-value and the R-free, calculated with 5% of the reflections. The overall quality of the final model was assessed by using the programs PROCHECK[112] and WHATIF[113, 114]. Visualization, analysis and figure

preparation were carried out with MolScript[115] and PyMOL (The PyMOL Molecular Graphics System, Version 1.5.0.1 Schrödinger, LLC).

3.1.5 Isothermal Titration Calorimetry

Binding of LmFPPS to four ligands: 1-(2-hydroxy-2,2-bis-phosphono-ethyl)-3-phenyl-pyridinium (300B); 1-(2,2-bis-phosphono-ethyl)-3-butyl-pyridinium (476A); 3-fluoro-l-(2-hydroxy-2,2-bis-phosphono-ethyl)-pyridinium (46I) and 1-hydroxy-2-imidazolyl-ethylidene-1,1-bisphosphonate monohydrate (91B; zoledronate)[6], was studied by isothermal titration calorimetry using a VP-ITC instrument (Microcal Inc, Northampton, MA). For these experiments the protein was diluted to 25 μM (based on the monomer MW) in a buffer containing 25 mM Hepes pH 7.5, 1 mM TCEP, 300 mM NaCl and 5 mM $MgCl_2$. Ligand solutions were prepared in the same buffer at a concentration of 250 μM. 1.4 mL of protein in the sample cell was titrated with 24, 10 μL injections after an initial 2 μL injection. The heat evolved at 28 °C after each ligand injection was obtained by integration of the calorimetric signal after subtracting the average heat of dilution. The data were analyzed with the Origin-5.0 software and fitted to a single binding site per monomer. (Table 3.)

3.1.6 Activity against *L. donovani* axenic amastigotes

Amastigotes of *L. donovani* strain MHOM/ET/67/L82 were grown in axenic culture at 37 °C in SM medium[116] at pH 5.4 supplemented with 10% heat-inactivated

fetal bovine serum under an atmosphere of 5% CO_2 in air. 100 □L of culture medium with 10^5 amastigotes from axenic culture with or without a serial drug dilution were seeded in 96-well microtitre plates. Serial drug dilutions of seven 3-fold dilution steps covering a range from 90 to 0.123 µg/mL were prepared. After 72 h of incubation the plates were inspected under an inverted microscope to evaluate growth of the controls under sterile conditions. 10 µL of Alamar Blue (12.5 mg resazurin dissolved in 100 mL distilled water) [117] were added to each well and the plates incubated for another 2 h. Plates were read with a Spectramax Gemini XS microplate fluorometer (Molecular Devices Cooperation, Sunnyvale, CA, USA) using an excitation wave length of 536 nm and an emission wave length of 588 nm. Data were analyzed using the software Softmax Pro (Molecular Devices Cooperation, Sunnyvale, CA, USA). Decrease of fluorescence (reporting inhibition) was expressed as percentage of the fluorescence of control cultures and plotted against the drug concentrations. IC_{50} values were calculated from the sigmoidal inhibition curves(Table 2.).

3.1.7 Activity against *L. donovani* intracellular amastigotes: macrophage assay

Mouse peritoneal macrophages (4 x 10^4 in 100 µL RPMI 1640 medium with 10% heat-inactivated FBS) were seeded into wells of Lab-tek 16-chamber slides. After 24 hrs 1.2 x 10^5 amastigote *Leishmania donovani* in 100 µL were added. The amastigotes were taken from an axenic amastigote culture grown at pH 5.4. Four hours later the medium containing free amastigote forms was removed and replaced by fresh medium. Next day, the medium was replaced by medium containing different compound dilutions. Parasite

growth in the presence of the drug was compared to control wells. After 96 hours of incubation the medium was removed and the slides fixed with methanol for 10 min followed by a staining with a 10% Giemsa solution. Control cultures and the ones exposed to the serial drug dilutions of infected and non-infected macrophages were counted. Infection rates were determined and the results expressed as the reduction in parasite burden compared to control wells, and the IC_{50} calculated by linear regression analysis.

3.2 Experimental Procedures: TcFPPS Project

3.2.1 Synthesis of inhibitors

Compounds BR6–BR28 were synthesized as reported before[97]. In brief; they were prepared using tetraethyl ethenylidene bisphosphonate as a Michael acceptor,[118] which in turn was prepared from tetraethyl methylenebisphosphonate in two steps according to a slightly modified Degenhart protocol[119]. The compound was reacted with the corresponding *n*-alkylamine *via* a 1,4-conjugated addition reaction to yield the respective Michael adducts. Once these synthetic precursors were at hand, they were hydrolyzed with bromotrimethylsilane in methylene chloride[120] to afford the free 1,1-bisphosphonic acids (**10**–**14**). The purity of the compounds assessed by elemental analysis was greater than 98%[97].

3.2.2 Cloning, Expression and Purification

TcFPPS was cloned and expressed as reported before[121]. Briefly, DNA coding for TcFPPS with an N-terminal His-Tag and a thrombin cleaveage site was cloned into a pET28a vector (Novagen). BL21(DE3) *E. coli* cells transformed with this plasmid were grown in LB medium until they reached an OD_{600} of 0.8 and induced with 0.1 mM IPTG at 37.0 ^{o}C. The cells were harvested 3h after induction, washed in buffer A (50 mM NaH_2PO_4 pH 8.0 300 mM NaCl, 10 mM imidazole, 1 mM TCEP; TCEP: tris(2-carboxyethyl) phosphine hydrochloride), and broken with a microfluidizer. The lysate was centrifuged for 30 mins at 12000 rpm and the supernatant was loaded onto a HisTrap Ni^{2+} chelate affinity column equilibrated with buffer A. The protein was eluted using a linear gradient of 0-100% of buffer B (50 mM NaH_2PO_4 pH 8.0 300 mM NaCl, 500 mM Imidazole, 1 mM TCEP). The His-tag was cleaved by digestion with thrombin and the sample was loaded into an anion exchange column (binding buffer: 20 mM Tris pH 8.2, 20 mM NaCl, 1 mM TCEP) and eluted with 20 mM Tris pH 8.2, 1 M NaCl, 1 mM TCEP. The protein, which was more than 95% pure as seen by SDS page gel, was dialyzed against 20 mM Tris pH 8.2, 150 mM NaCl, 1 mM TCEP and concentrated to 12 mg mL^{-1}.

3.2.3 Crystallization

Crystals used for data collection were grown by vapor diffusion with the protein and the mother liquor in a 1:1 ratio. The reservoir consisted of 100 mM sodium acetate, pH 4.6–5.2, 200 mM ammonium sulfate, and 2–10% PEG 4K. Crystals, which appear within 1-2 days, belong to the hexagonal space group $P6_122$. The protein (12.5 mg/ml)

inhibitor solution used for co-crystallization contained 250 μM inhibitor, 250 μM IPP and 1 mM $MgCl_2$.

3.2.4 Data Collection

Diffraction data of all the TcFPPS complexes were collected at beamline X6A of the NSLS, Brookhaven National Laboratory. Diffraction data collected from a single frozen crystal (100 K) were processed and scaled using the HKL 2000 suite[105] (Table 4).

3.2.5 Structure Determination

The structures of the complexes of TcFPPS with compounds BR11, BR18, BR6 and BR28 were determined by direct refinement of the coordinates of the FPPS from Trypanosoma cruzi (1YHM)[7] with the program REFMAC5[108, 109, 122] of CCP4 suite. The structure of BR25 was determined by molecular replacement using the program AMoRe[106] (search molecule PDB id 1YHM).

3.2.6 Model Building and Refinement

The initial model was refined using REFMAC5 and rebuilt during refinement with the program COOT[111]. The R-value and the R-free, calculated with a cross validation set containing 5% of the reflections, were used to monitor progress of the refinement. The overall quality of the final model was assessed using the programs

PROCHECK[112] and WHATIF[113, 114]. Atomic coordinates and structure factors for the complexes TcFPPS+BR25, TcFPPS+BR6, TcFPPS+BR18, TcFPPS+BR11 and TcFPPS+BR28 have been deposited in the Protein Data Bank with accession codes 4DWB, 4DXJ, 4DWG, 4EIE and 4DZW respectively. Structure figures were generated using molscript[115] and pymol (The PyMOL Molecular Graphics System, Version 1.5.0.1 Schrödinger, LLC). Models of the proposed new inhibitors were built using MOE (Molecular Operating Environment, Quebec, Canada).

3.2.7 Isothermal Calorimetry

ITC experiments were performed with TcFPPS and each of five ligands: BR6, BR25, BR18, BR11 and BR28. The protein was diluted to a concentration of 29 μM (in monomers) in a buffer containing 25 mM Hepes pH 7.5, 1 mM TCEP, 300 mM NaCl, 2 mM $MgCl_2$. The ligands were prepared in the same buffer at a concentration of 250 μM. 1.3 mL of protein in the sample cell were titrated with twenty five 10 μl injections. The data were analyzed with the Origin-5.0 software and fitted to a single binding site per monomer. (A two-site per dimer was also used for BR11.) (Table 5.)

4. Appendix I: Genetic Engineering of the protein LmFPPS to produce a mixture of GPP and FPP

4.1 Introduction

Farnesyl Pyrophosphate Synthase is an enzyme of the mevalonate pathway, a metabolic pathway that takes Acetyl-CoA from the citric acid cycle to synthesize isoprenoids. FPP Synthase takes two 5-carbon molecules, isoprenyl pyrophosphate (IPP) and dimethylallyl pyrophosphate (DMAPP), and in a two-step condensation process produces farnesyl pyrophosphate (FPP), a 15-carbon molecule[45]. Geranyl pyrophosphate (GPP) is a 10-carbon molecule product of the first condensation that quickly gets condensed with another IPP to become FPP. FPP is further used in several different metabolic pathways, including membrane and steroid synthesis.

One key motif that is found in all of the FPP synthases is DDXX(XX)D, where X is any amino acid. Depending on the species, there can be two residues between the aspartates (eukaryotic FPP synthases), or four residues (bacterial FPP synthases). In addition, all eukaryotic FPP synthases have two aromatic amino acids at fourth and fifth positions before the first aspartate rich motif (FARM) DDXXD. Similarly, bacterial FPP synthases have one aromatic amino acid at the fifth position before DDXXXXD motif.

Our group recently determined the structure of the wild type *Leishmania major* FPPS, and based on its crystal structure, residues were identified around the active site which, when mutated to a bulky amino acid, could inhibit the production of FPP and force the reaction to stop at the production of GPP. FPP, being a 15-carbon molecule, is longer than GPP, and if the tunnel where both GPP and FPP bind is shortened, the formation of FPP could be diminished simply because the active site is not long enough to accommodate a 15-carbon molecule, in turn stopping the catalysis at the production of

GPP. Four such residues were proposed: Leu129, Asn126, Thr164 and Glu97. We hypothesized that each residue, if mutated to bulky amino acid, would form a cap in the middle of the tunnel and shorten the length of the active site.

In addition, we designed an insertion mutant with two extra residues in between the aspartates residues of the first aspartate rich motif (FARM). Narita et al. have previously demonstrated with *Bacillus stearothermophilus* FPPS that it is possible to alter the product specificity (convert FPPS into GPPS) by mutating the non-aromatic amino acid at 4^{th} position before DDXXXXD motif into an aromatic amino acid[59]. To see whether this is also applicable to eukaryotic FPPS, we decided to test whether it is possible to convert L. major FPPS (which already has aromatic amino acids at 4^{th} and 5^{th} position before DDXXD motif) into GPPS by inserting two residues in between its DDXXD motif.

4.2 Experimental Procedures and Materials

4.2.1 Materials

^{14}C labeled Isopentenyl pyrophosphate was custom ordered from PerkinElmer (Waltham, MA). TLC plates were ordered from Whatman (Florham Park, NJ). DMAPP, IPP and GPP were purchased from Sigma-Aldrich.

4.2.2 Cloning and design of mutants

L. major FPPS was cloned into a pET-28a vector as described previously[103]. Briefly, DNA coding for LmFPPS (with an N-terminal His-Tag and a thrombin cleavage site) was cloned into a pET28a vector (Novagen). All mutants were generated using the QuikChange site-directed mutagenesis kit (Strategene). Forward and reverse primers for the mutations are in the Table 6. The PCR products were used to transform GC5 cells for storage and to BL21 for expression. Isolated plasmid DNA from transformed colonies was sequenced.

Primer name	Sequence (5'-3')
L129F_F	CCATCAATGACGGTTTCATTCTGCTGGCC
L129F_R	GGCCAGCAGAATGAAACCGTCATTGATGG
L129Y_F	CCATCAATGACGGTTACATTCTGCTGGCCTG
L129Y_R	CAGGCCAGCAGAATGTAACCGTCATTGATGG
L129W_F	GCCATCAATGACGGTTGGATTCTGCTGGCCTGG
L129W_R	CCAGGCCAGCAGAATCCAACCGTCATTGATGGC
T164F_F	GACGTCGATCTCACTACCTTTATTGGTCAGCTGTACGAC
T164F_R	GTCGTACAGCTGACCAATAAAGGTAGTGAGATCGACGTC
T164W_F	CGTCGATCTCACTACCTGGATTGGTCAGCTGTAC
T164W_R	GTACAGCTGACCAATCCAGGTAGTGAGATCGACG
T164Y_F	GACGTCGATCTCACTACCTATATTGGTCAGCTGTACGAC
T164Y_R	GTCGTACAGCTGACCAATATAGGTAGTGAGATCGACGTC
E97F_F	GGCCCACTTCCTTGTGTTTGACGACATCATGGACC
E97F_R	GGTCCATGATGTCGTCAAACACAAGGAAGTGGGCC
E97W_F	CCCACTTCCTTGTGTGGGACGACATCATGG
E97W_R	CCATGATGTCGTCCCACACAAGGAAGTGGG
E97Y_F	GGCCCACTTCCTTGTGTATGACGACATCATGGACC
E97Y_R	GGTCCATGATGTCGTCATACACAAGGAAGTGGGCC
N126W_F	CAGGTGGCCATCTGGGACGGTCTCATTCTG
N126W_R	CAGAATGAGACCGTCCCAGATGGCCACCTG
N126Y_F	CGCAGGTGGCCATCTATGACGGTCTCATTC
N126Y_R	GAATGAGACCGTCATAGATGGCCACCTGCG
MD101insPS_F	CTTGTGGAGGACGACATCCCGAGCATGGACCACAG
MD101insPS_R	CTGTGGTCCATGCTCGGGATGTCGTCCTCCACAAG

Table 6. List of primers used in generating LmFPPS mutants.

4.2.3 Expression and Purification

LmFPPS was expressed as reported previously[103]. Briefly, plasmid DNA was used to transform *E. coli* BL21(DE3) cells. BL21(DE3) *E. coli* cells transformed with this plasmid were grown in LB medium until they reached an OD_{600} of 0.8 and were then induced with 0.1 mM IPTG at 37 ^{o}C. Cells were harvested 3h after induction and were washed in buffer A (50 mM NaH_2PO_4 pH 8.0 300 mM NaCl, 10 mM imidazole, 1 mM TCEP). After the cells were broken with a micro-fluidizer, the lysate was centrifuged for 30 minutes at 12000 rpm, and the supernatant loaded onto a HisTrap Ni^{2+} chelate affinity column equilibrated with buffer A. Protein was eluted using a linear gradient of 0-100% of buffer B (50 mM NaH_2PO_4 pH 8.0 300 mM NaCl, 500 mM imidazole, 1 mM TCEP). The poly-histidine tag was cleaved by digestion with thrombin, and the sample loaded onto an anion exchange column (binding buffer: 20 mM Tris pH 8.2, 50 mM NaCl, 1 mM TCEP) and eluted with 20 mM Tris pH 8.2, 1 M NaCl, 1 mM TCEP. The eluate was further purified through a second round of nickel affinity chromatography, collecting the flow through. The protein was dialyzed against 20 mM Tris pH 8.2, 150 mM NaCl, 1 mM TCEP and concentrated to 15 mg/mL.

4.2.4 Radioactive Assay of Mutant LmFPPS

Six 350 µl reaction mixtures were prepared, each containing increasing amount of DMAPP: 1 mM, 5 mM, 25 mM, 50 mM, 100 mM and 400 mM. Each reaction mixture contained 100 mM Tris-HCl, pH 7.5, 1 mM $MgCl_2$, 1 mM TCEP and 100 µM IPP. The mixtures were placed on 25 °C. 50 µl was taken from each reaction mixture for the 0-

minute time point and hydrolyzed with 10 µl of 6 M HCl. Reactions were initiated by adding 350 ng of enzyme. 50 µl was taken out every 1 minute and hydrolyzed. 50 µl samples were neutralized subsequently with 10 µl of 6 M NaOH. The samples were then mixed with saturated butanol, and then with saturated NaCl to extract the hydrolyzed products. 500 µl was taken from each butanol layer and mixed with scintillation cocktail for counting.

4.2.5 TLC Analysis of the Products

500 µl reaction mixtures were prepared, each containing 200 mM Tris, pH 8.0, 10 mM $MgCl_2$, 1 mM TCEP, 100 µM ^{14}C-IPP, 50 µM DMAPP, and 140 µg of corresponding enzyme. The mixtures were initially incubated at 37°C for 3 hours, and afterwards 1 µl of Bacterial Alkaline Phosphatase (150 U/µl) were added to the mixtures and further incubated overnight. They were then extracted with 2 ml of hexane, and the hexane layers were concentrated until the volume was down to about 100 µl. The concentrated extracts were then blotted on TLC plate, along with standard geraniol and farnesol. The plate was run in benzene:ethyl acetate (4:1) solvent and developed with iodine vapor. Radio-labeled solution was blotted on iodine spots for geraniol and farnesol standards to visualize the spots in phosphorimager. The plate was then exposed to phosphorimager screen and subsequently analyzed.

4.2.6 Crystallization of Mutant LmFPPS

Crystals of mutant LmFPPS Thr164Tyr and Glu146Tyr FPPS were grown by hanging drop vapor diffusion at 20° C with 1 mL reservoirs buffer consisting of 0.1 M MES-sodium salt, 15-25% PEG 8000 and 0.1-0.2 M calcium acetate. Each drop contained 1 μl of reservoir solution and 1 μl of protein mixture at a concentration of 12 mg/ml in 50 mM Tris pH 8.0, 150 mM NaCl, 1 mM TCEP buffer with 0.4 mM IPP, 1 mM $MgCl_2$ and 0.4 mM of 476A.

4.2.7 Data collection and structure determination

Data from the FPPS mutant crystals were collected with a FR-e generator (Rigaku) as the source of X-rays on an R-AXIS IV image plate detector at the X-ray facility of the Department of Biophysics and Biophysical Chemistry of the Johns Hopkins University School of Medicine (Table 7). Data were indexed, integrated and scaled using HKL 2000 Suite. Structures were determined by Fourier synthesis using the Leishmania major farnesyl diphosphate synthase in complex with 476A as initial model. Model building and refinement were carried out iteratively using the programs COOT and REFMAC. Refinement statistics for both datasets are given in Table 7.

4.2.8 Small/wide-angle X-ray Scattering (SAXS/WAXS) of Leu129Trp LmFPPS.

Wild type and Leu129Trp LmFPPS x-ray scattering data were collected at the National Synchrotron Light Source BNL beamline X9 to assess the structural basis of the

differences in enzymatic activity. Scattering intensity data were collected at 4 mg/ml in buffer Y in triplicates and averaged after normalization and buffer extraction[123]. Data analysis was performed using the ATSAS software suite. Data was processed with the program PRIMUS[124] and regularized using GNOM[125, 126]. Calculated scattering plots from CRYSOL[127] using the wild type LmFPPS showed excellent agreement with crystallographic structure. The low resolution envelopes of Leu129Trp LmFPPS and wt LmFPPS were reconstructed from the scattering data ab initio using the promas DAMMIN[128] and DAMAVER[129]. Ten independent runs were averaged with the program DAMAVER.

Table 7. Data Collection and Refinement Statistics of the LmFPPS mutants

Crystal	T164Y + 476A + IPP	T164W + 476A + IPP	E97Y + 476A + IPP
Space group	$P2_12_12_1$	$P2_1$	$P2_12_12_1$
Cell dimensions	a = 80.5 Å	a = 58.9 Å	a = 80.7 Å
	b = 85.9 Å	b = 79.9 Å	b = 86.1 Å
	c = 107.2 Å	c = 81.2 Å	c = 107.4 Å
	α=b=γ = 90°	α=b=γ = 90°	α=b=γ = 90°
Data Collection Statistics			
X-ray Source	FRE-Raxis IV	FRE-CCD Saturn	FRE-CCD Saturn
Wavelength(Å)	1.54	1.54	1.54
Resolution(Å)	50.0-1.85	50.0-2.1	50.0-2.05
(HighRes shell)[a]	(1.92-1.85)	(2.18-2.10)	(2.09-2.05)
Measured Reflect.	412,194	123,691	201,477
Unique Reflections	63,800	38,828	43,443
I/σ	32.2 (2.5)	26.1 (5.3)	19.92 (3.84)
Completeness (%)	99.2 (92.8)	92.1 (57.8)	90.6 (78.7)
R_{sym} (%)[b]	8.0 (46.4)	7.2 (21.7)	7.7 (24.1)
Refinement			
R_{cryst}	0.196	0.184	0.229
R_{free}	0.2295	0.238	0.307
R.m.s deviations & Number of atoms			
Bond length (Å)	0.008	0.009	0.016
Angle (°)	1.044	1.165	1.821
Monomer in ASU	2	2	2
Total Atoms	6603	6387	5832
Protein atoms	5812	5848	5772
Water molecules	701	448	449

[a]Data in parentheses belong to the outer resolution shell.

[b]$R_{merge}=\sum_{hkl}\sum_J|I_J-\langle I\rangle|/\sum_{hkl}\sum_J I_J$ where $\langle I\rangle$ is the mean intensity of J observations from a reflection hkl and its symmetry equivalents.

4.3 Results

4.3.1 Kinetics Assay

After the enzymatic reaction with DMAPP and IPP as substrates, HCl is added to hydrolyze the pyrophosphates of the products FPP and GPP, subsequently converting them into farnesol and geraniol, respectively. However, as both DMAPP and IPP are acid stable and do not get hydrolyzed into alcohols. Hence, only the hydrolyzed products are extracted into the hexane layer and are detected by the scintillation counter.

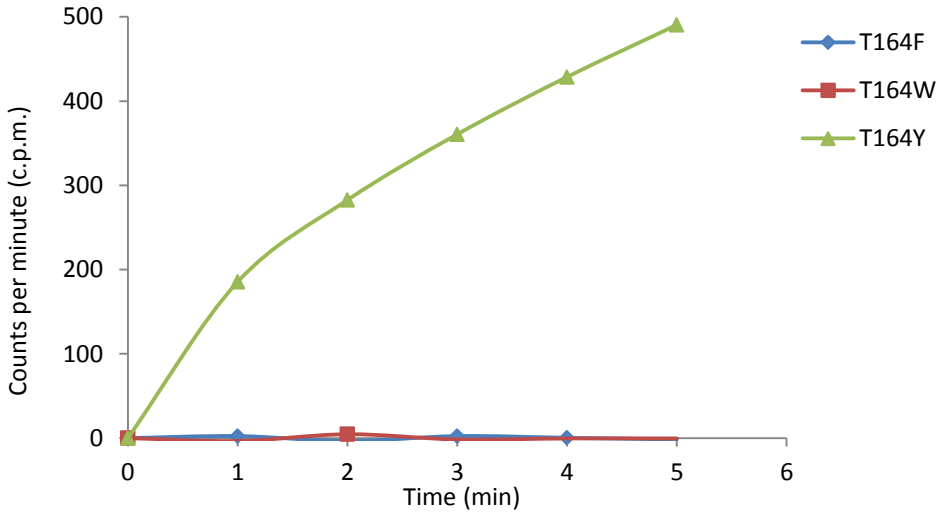

Figure 22. Kinetic studies of the three mutants T164F, T164W and T164Y.

Amount of product formed by the three mutants and the wildtype LmFPPS from substrates DMAPP and IPP. The amount of products formed by T164Y mutant is more than twice the amount of products formed by the wild type LmFPPS. Both T164F and T164W mutants are inactive.

We first observed the initial reaction rates of the three Thr164 mutants by carrying out the reaction with 100 µM IPP and 50 µM DMAPP. Out of the three mutants Thr164Phe, Thr164Trp and Thr164Y, only Thr164Tyr mutant was active (Fig. 22). However, 'counts per minute' do not tell us what kind of product the mutant produced. Since the substrates were IPP and DMAPP, the reaction could have stopped at the formation of GPP, or the enzyme could have converted all the substrates to FPP.

We performed another experiment to find out whether Thr164Tyr mutant can produce FPP or not. We conducted another kinetics assay with 100 µM IPP and 50 µM GPP to limit FPP as the only possible product. The result showed a linear increase in

counts for Thr164Tyr mutant (Fig. 23), indicating that Thr164Tyr mutant produces FPP. In addition, the amount of FPP formed by Thr164Tyr mutant was more than two times greater than the amount of FPP formed by the wild type LmFPPS.

We further performed Michaelis-Menten kinetics assay for Thr164Tyr and the wild type, with IPP and DMAPP as substrates. The graph showed that although K_M for both enzymes were almost identical, V_{max} of the mutant (166.312 cpm/min) was about 42% greater than that of the wild type (117.504 cpm/min) (Fig. 22.). The result shows that the Thr164Tyr mutant is in fact more efficient than the wild type in synthesizing FPP from IPP and DMAPP.

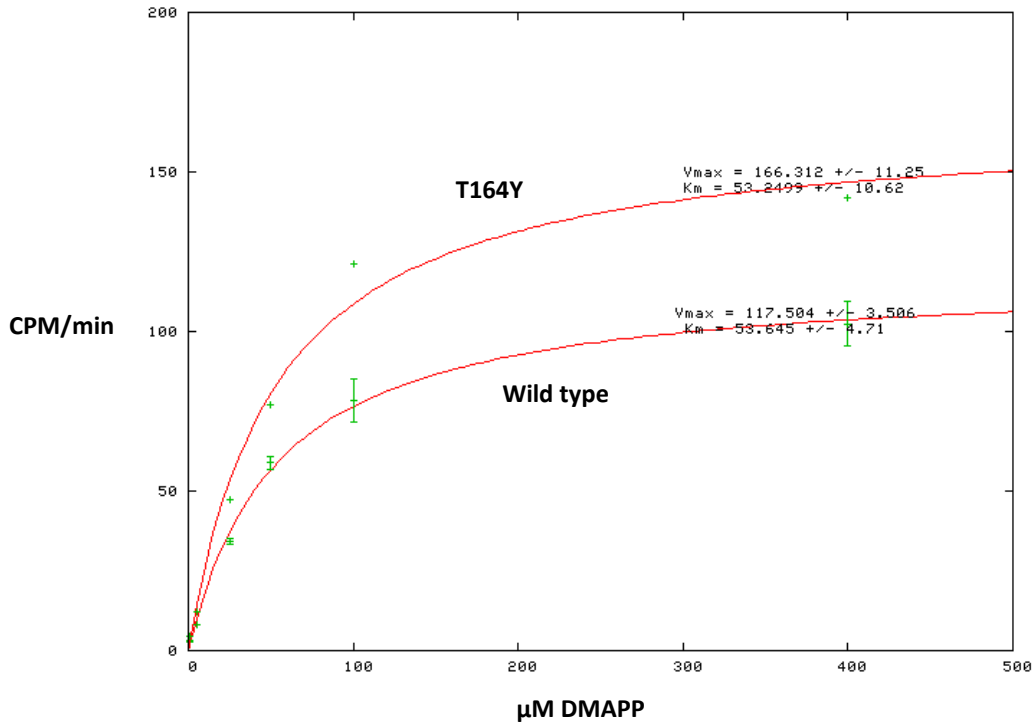

Figure 23. Michaelis-Menten Kinetics data for the mutant T164Y and wild type LmFPPS

K_M for both the mutant and wild-type is in the same range. On the other hand, v_{max} for T164Y is 166.312 CPM/min, 42 % greater than V_{max} for the wild type (117.504 CPM/min).

4.3.2 Thin Layer Chromatography

Results from the kinetic assays revealed that Thr164Tyr mutant is capable of producing FPP, and also do it more efficiently than the wild type. However, they still do not tell us about whether the mutant can produce only FPP, or a mixture of FPP and GPP. In order to find out, we hydrolyzed the product from enzymatic reactions and blotted the solution on TLC plate. The result showed two distinct spots on Thr164Tyr mutant lane.

The two spots corresponded to the two standard spots (geraniol and farnesol), indicating that Thr164Tyr mutant is capable of synthesizing GPP as well as FPP. As expected, the wild type only produced FPP as product, which can be seen from the TLC plate with only one spot visible that corresponds to farnesol (Fig. 24).

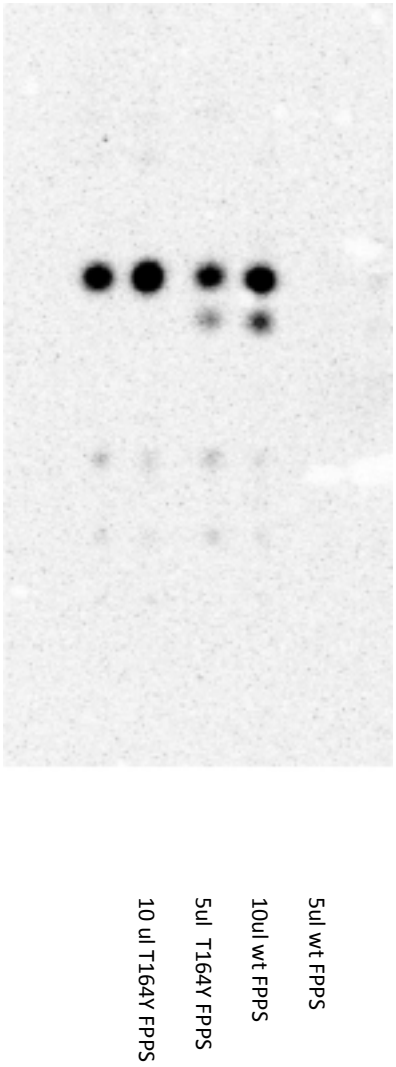

Figure 24. TLC analysis of the hydrolyzed products obtained from the mutant T164Y and wt-LmFPPS.

Phosphorimager scan of the TLC plate with hydrolyzed products obtained from the mutant T164Y and the wild type LmFPPS. Two spots, each corresponding to geraniol and farnesol, are visible on both T164Y lanes. This proves that T164Y mutant can synthesize both FPP and GPP as products. The spots on the TLC plate were first visualized with iodine vapor. Since stock geraniol and farnesol are not radio-labeled, we blotted a small amount of ^{14}C-labeled IPP on the two standards, after they were visualized with iodine.

We further expanded the experiment to cover all the mutants that were prepared (Fig. 25). No spots were visualized on Thr164Phe, Thr164Trp – as expected from the kinetics assay results – and insertion mutant. In addition, we observed that all Glu97 and Asn126 mutants behaved like the wild type, producing FPP as the only product (Fig. 25). From this analysis we can conclude that out of all the LmFPPS mutants studied, only Thr164Tyr showed activity towards the production of both FPP and GPP.

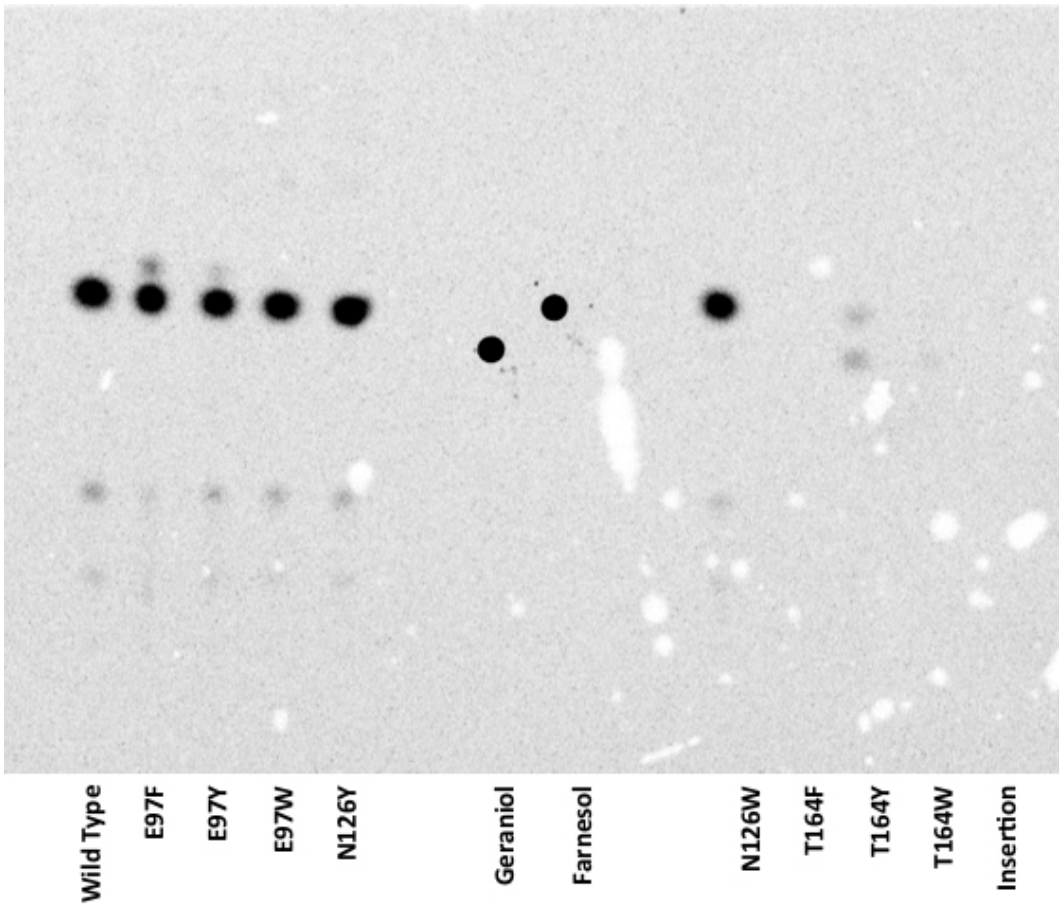

Figure 25. TLC analysis of the products obtained from all the mutants used in the study.

Phosphorimager scan of the TLC plate with hydrolyzed products obtained from all mutants and the wild type LmFPPS. T164Y is the only mutant that has two spots visible at geraniol and farnesol. Other mutants show no visible spots (T164F, T164W and insertion), or look like the wild type with only one spot visible at farnesol (E97 and N126 mutants).

4.3.3 Crystallography

From the thirteen mutants originally constructed, we crystallized three mutants: Glu97Tyr, Thr164Trp and Thr164Tyr. The crystals formed when the reservoir contained 20 – 25 % PEG 8000, 100 – 200 mM Ca acetate, and 100 mM MES NaCl pH 6.5. Wild type *Lm*FPPS was crystallized with IPP and the inhibitor 300B in the active site, but the mutants were crystallized with IPP and the inhibitor 476A since 476A is longer than 300B and thus can have closer interaction with the mutated residues at the bottom of the active site. Both Glu97Tyr and Thr164Tyr mutants crystallized in primitive orthorhombic space group ($P2_12_12_1$), with unit cell dimensions of a ≈ 80.6 Å, b ≈ 86 Å, c ≈ 107 Å, and α=β=ϒ= 90°. The crystal of Thr164Trp had primitive monoclinic space group ($P2_1$), with unit cell dimensions of a ≈ 59 Å, b ≈ 80 Å, c ≈ 81 Å, and α=β=ϒ= 90°. We refined Thr164Tyr to 1.85 Å, Thr164Trp to 2.1 Å and Glu97Tyr to ~ 2.05Å (Table 7).

5. Appendix II: Expression, Purification and Thermodynamic studies of Trypanosoma Cruzi Solanesyl Diphosphate Synthase

5.1 Experimental Procedures

5.1.1 Cloning, expression and purification

TcSPPS was cloned and expressed after pruning first 8 residues as reported previously[130]. Briefly, DNA coding for TcSPPS (with an N-terminal His-Tag and a thrombin cleavage site) was cloned into a pET28a vector (Novagen). BL21(DE3) *E. coli* cells transformed with this plasmid were grown in LB medium until they reached an OD_{600} of 0.8 and were then induced with 0.1 mM IPTG at 37 ^{o}C. Cells were harvested 3h after induction and were washed in buffer A (50 mM NaH_2PO_4 pH 8.0 300 mM NaCl, 10 mM imidazole, 1 mM TCEP, 10% glycerol). After the cells were broken with a micro-fluidizer, the lysate was centrifuged for 30 minutes at 12000 rpm, and the supernatant loaded onto a HisTrap Ni^{2+} chelate affinity column equilibrated with buffer A. Protein was eluted using a linear gradient of 0-100% of buffer B (50 mM NaH_2PO_4 pH 8.0 300 mM NaCl, 500 mM imidazole, 1 mM TCEP, 10% glycerol). The poly-histidine tag was cleaved by digestion with thrombin, and the sample loaded onto an anion exchange column (binding buffer: 20 mM Tris pH 8.2, 50 mM NaCl, 1 mM TCEP, 10% glycerol) and eluted with 20 mM Tris pH 8.2, 1 M NaCl, 1 mM TCEP and 10% glycerol. The eluate was further purified through a second round of nickel affinity chromatography, collecting the flow through. The protein was dialyzed against 20 mM Tris pH 8.2, 150 mM NaCl, 1 mM TCEP, 10% glycerol and concentrated to 10 mg/mL. Protein when run through Gel exclusion column S-200 it comes of as a monodisperse dimer.

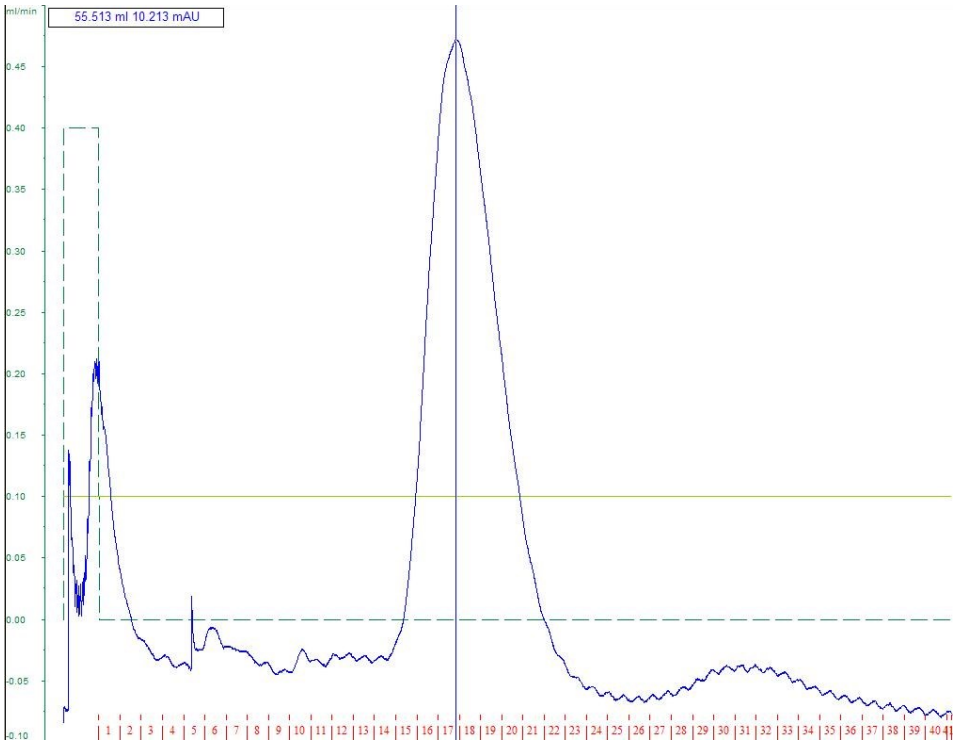

Figure 26. Size exclusion chomatography of the purification of the TcSPPS.

5.1.2 Crystallization attempts

A full search of crystallization conditions was carried out using an incomplete factorial set of conditions[104]. Initial hits were seen in the condition 200 mM Na Citrate pH 5.5, 16% w/v PEG 8000. The crystal diffracted to approximately 6 Å and they were obtained using the microseeding technique. The protein (10 mg/ml) solution used for crystallization contained 25 mM Na citrate pH 5.0, 25 mM NaCl, 10% glycerol, 1 mM TCEP.

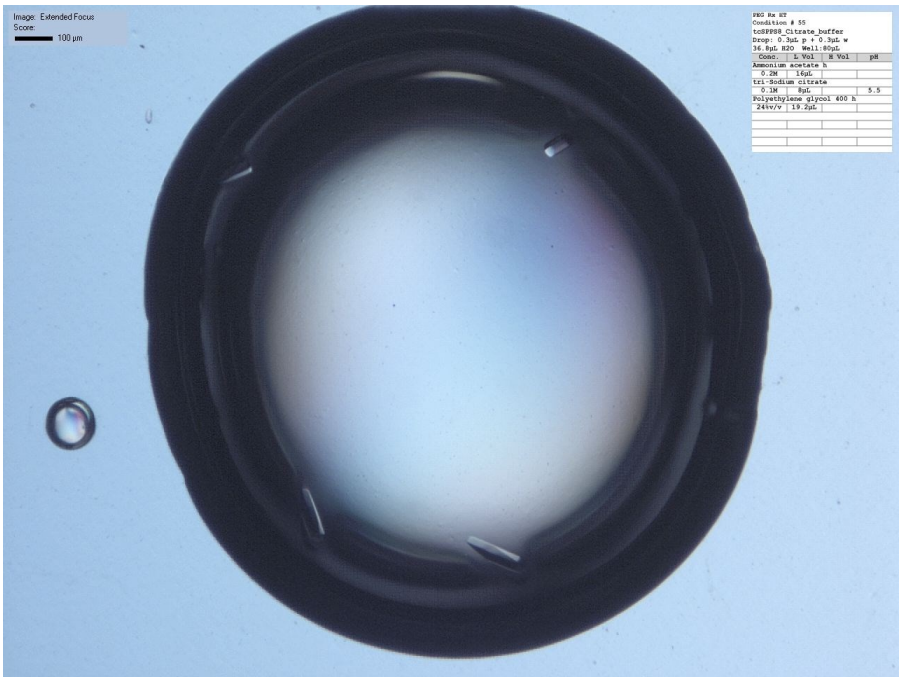

Figure 27. Crystals of TcSPPS.

5.1.3 Isothermal Titration Calorimetry

Binding of TcSPPS to the bisphosphonates: BR6, BR25, BR18, BR11 and BR28 were studied by isothermal titration calorimetry using a VP-ITC instrument (Microcal Inc, Northampton, MA). For these experiments the protein was diluted to 25 µM (based on the monomer MW) in a buffer containing 25 mM Hepes pH 7.5, 1 mM TCEP, 300 mM NaCl, 10% glycerol and 5 mM $MgCl_2$. Ligand solutions were prepared in the same buffer at a concentration of 250 µM. 1.4 mL of protein in the sample cell was titrated with 24, 10 µL injections after an initial 2 µL injection. The heat evolved at 28 °C after each ligand injection was obtained by integration of the calorimetric signal after subtracting the average heat of dilution. The data were analyzed with the Origin-5.0 software and fitted to a single binding site per monomer.

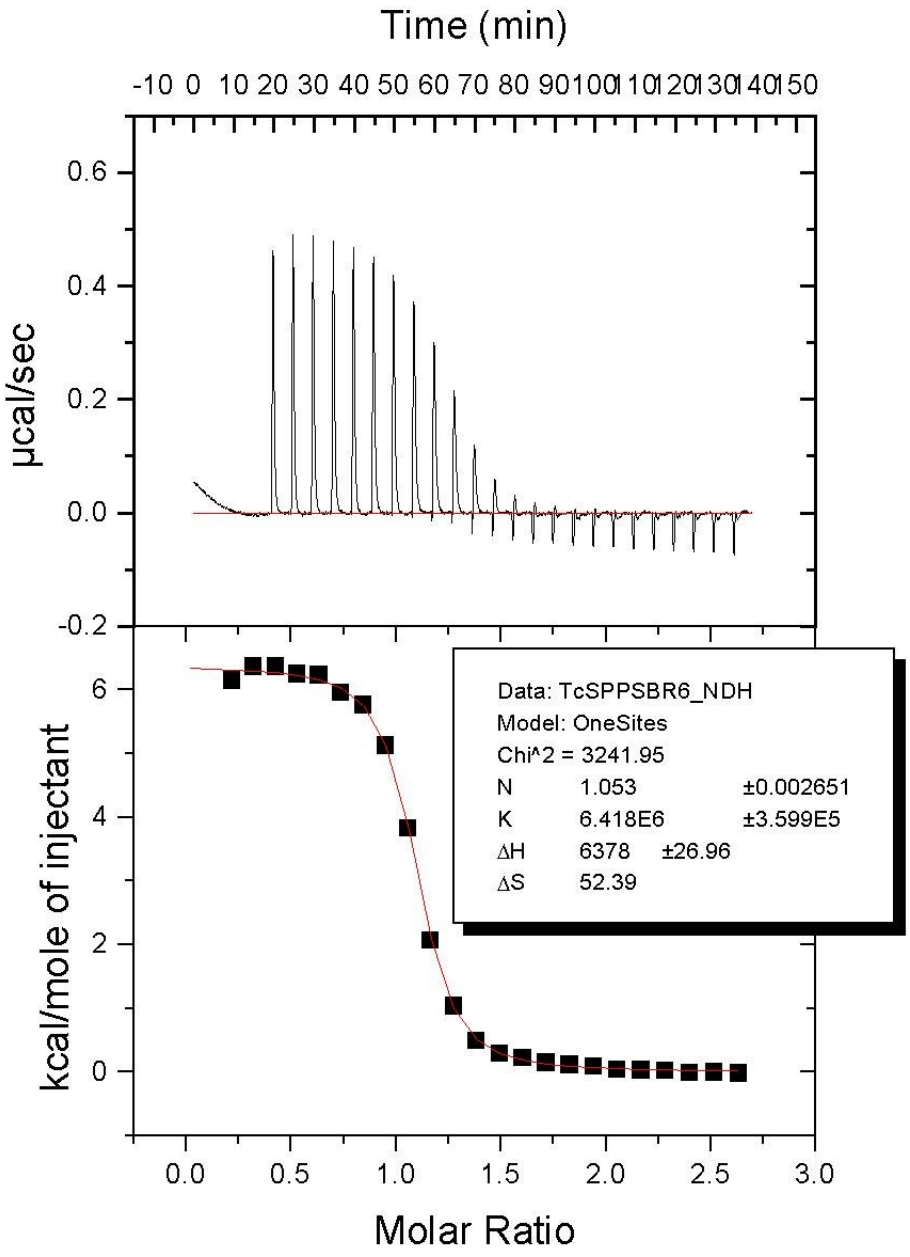

Figure 28. Isothermal calorimetry studies of BR6 and TcSPPS binding.

6. Appendix III: Purification and thermodynamic studies of the interaction between $Na_v1.5$ Channel C-terminal Domain and Calmodulin

6.1 Experimental Procedures

6.1.1 Cloning, expression and purification

The C- terminus of the alpha isoform of the $Na_v1.5$ channel, accession number NP_001092874, amino acids 1782-1929 ($CtNa_v1.5$) was inserted into the PGEX-6-P1 vector, which contains a GST tag, to express the fusion protein. The plasmid was co-transformed with calmodulin (CaM) previously inserted into another plasmid pET 24b. After expression, the $CtNa_v1.5$/CaM complex was purified using affinity chromatography to bind the GST fusion protein to GST resin and eluted using reduced glutathione. The size of the fusion protein GST+CtNaC is 45 kDa, that of GST is 27 kDa and that of CaM 16 kDa.

After initial elution of around 15 mg of protein per 4 L culture, the pellet was washed overnight and resolubilized material was subjected to another step of affinity purification with glutathione to recover 15 more mg of protein. A total of 30 mg of GST-CtNaC/CaM was recovered from 4 L. 0.3 mg of precission protease was added to the GST-CtNaC/CaM per 10 mg of protein. The protein was dialyzed overnight against 50 mM Tris pH 7, 1 mM DTT. The next day, protein was loaded onto a SourceQ column using mixtures of 50 mM Tris pH 7, 1 mM DTT as buffer A and 50 mM Tris pH 7, 1 mM DTT, 1 M NaCl as buffer B. The column was equilibrated with 5% buffer B and 95% buffer A. The protein was loaded and the column was washed with 2 column volumes of 5% buffer B. A gradient of 5% to 10% buffer B over 2 CV was run over the column.

Next, a gradient of 10% to 35% buffer B was run over 20 CV. Lastly, a gradient of 35% to 100% buffer B was run over 2 CV.

6.1.2 Isothermal calorimetric studies

Binding of $Na_v1.5$ to CaM was studied by isothermal titration calorimetry using a VP-ITC instrument (Microcal Inc, Northampton, MA). For this experiment the protein was diluted to 75 μM (based on the monomer MW) in a buffer containing 10 mM Na_2HPO_4 pH 7.4, 2 mM K_2HPO_4, 1 mM TCEP, 137 mM NaCl, 2.7 mM KCl, 10% glycerol and 5 mM $MgCl_2$. CaM was prepared in the same buffer at a concentration of 1 mM. 1.4 mL of protein in the sample cell was titrated with 24, 10 μL injections after an initial 2 μL injection. The heat evolved at 27 °C after each ligand injection was obtained by integration of the calorimetric signal after subtracting the average heat of dilution. The data were analyzed with the Origin-5.0 software and fitted to a single binding site per monomer.

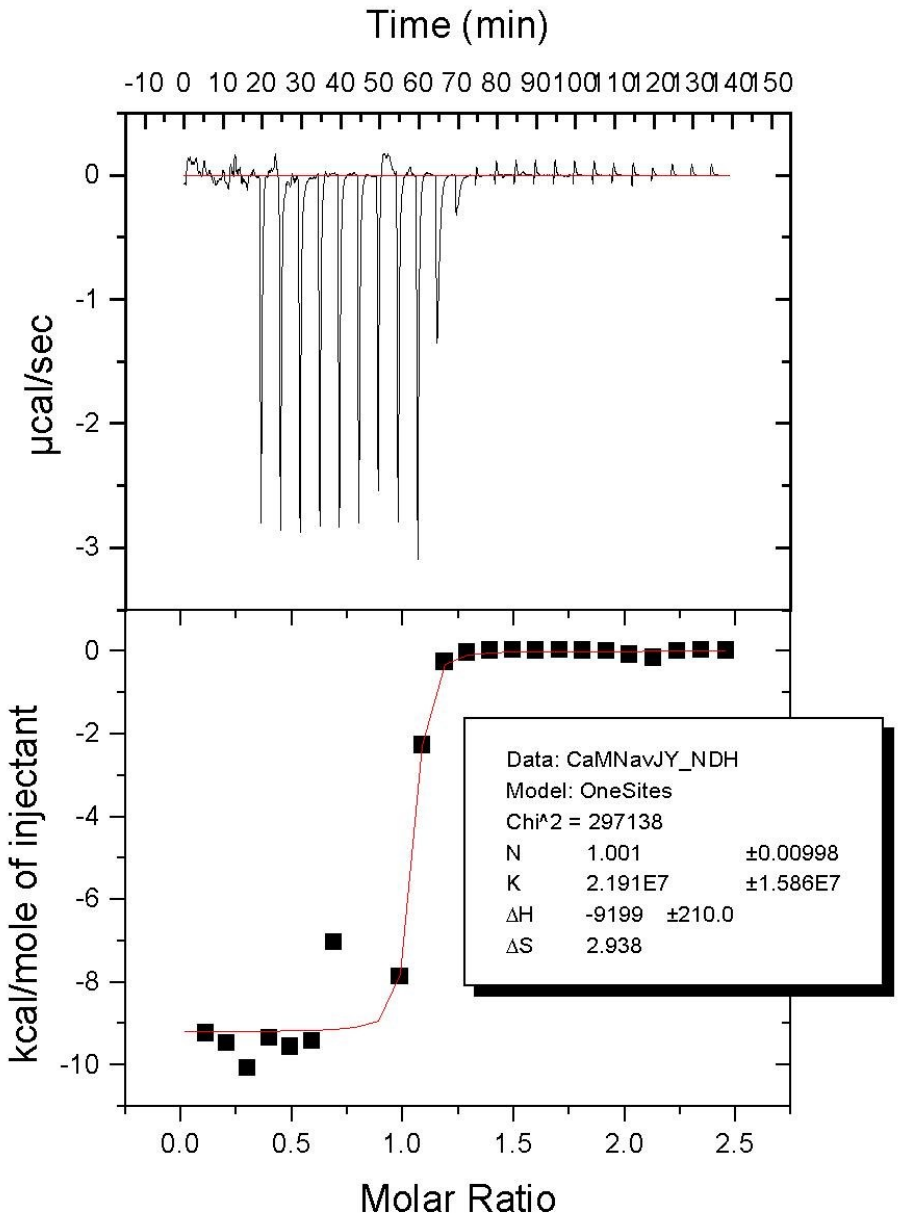

Figure 29. ITC studies of $Na_v1.5$ and CaM binding.

Bibliography

1. Molyneux DH, Malecela MN: **Neglected Tropical Diseases and the Millennium Development Goals - why the "other diseases" matter: reality versus rhetoric**. *Parasit Vectors*, **4**(1):234.
2. Kristjansson J, Gudmundsson S: **[Neglected tropical diseases - review]**. *Laeknabladid*, **97**(12):693-697.
3. Departamento de Ciencia e Tecnologia SdC, Tecnologia e Insumos Estrategicos, Ministerio da Saude.: **Doencas negligenciadas: estrategias do Ministerio da Saude.** *Rev Saude Publica* 2010, **44**(1):200-202.
4. Pontes Fv: **Doenças negligenciadas ainda matam 1 milhão por ano no mundo.** *Inovação em Pauta* 2010:69-73.
5. Croft SL: **Neglected diseases: progress in drug development**. *Curr Opin Investig Drugs* 2007, **8**(2):103-104.
6. Huang CH, Gabelli SB, Oldfield E, Amzel LM: **Binding of nitrogen-containing bisphosphonates (N-BPs) to the Trypanosoma cruzi farnesyl diphosphate synthase homodimer**. *Proteins* 2010, **78**(4):888-899.
7. Gabelli SB, McLellan JS, Montalvetti A, Oldfield E, Docampo R, Amzel LM: **Structure and mechanism of the farnesyl diphosphate synthase from Trypanosoma cruzi: implications for drug design**. *Proteins* 2006, **62**(1):80-88.
8. Robertson SA, Renslo AR: **Drug discovery for neglected tropical diseases at the Sandler Center**. *Future Med Chem*, **3**(10):1279-1288.
9. Birkholtz LM, Williams M, Niemand J, Louw AI, Persson L, Heby O: **Polyamine homoeostasis as a drug target in pathogenic protozoa: peculiarities and possibilities**. *Biochem J* 2011, **438**(2):229-244.
10. Chappuis F, Sundar S, Hailu A, Ghalib H, Rijal S, Peeling RW, Alvar J, Boelaert M: **Visceral leishmaniasis: what are the needs for diagnosis, treatment and control?** *Nat Rev Microbiol* 2007, **5**(11):873-882.
11. Rijal S, Yardley V, Chappuis F, Decuypere S, Khanal B, Singh R, Boelaert M, De Doncker S, Croft S, Dujardin JC: **Antimonial treatment of visceral leishmaniasis: are current in vitro susceptibility assays adequate for prognosis of in vivo therapy outcome?** *Microbes Infect* 2007, **9**(4):529-535.
12. Berman J: **Visceral leishmaniasis in the New World & Africa**. *Indian J Med Res* 2006, **123**(3):289-294.
13. Cuervo P, Domont GB, De Jesus JB: **Proteomics of trypanosomatids of human medical importance**. *J Proteomics* 2009, **73**(5):845-867.
14. Lainson R, Ready PD, Shaw JJ: **Leishmania in phlebotomid sandflies. VII. On the taxonomic status of Leishmania peruviana, causative agent of Peruvian 'uta', as indicated by its development in the sandfly, Lutzomyia longipalpis**. *Proc R Soc Lond B Biol Sci* 1979, **206**(1164):307-318.
15. Lainson R, Ward RD, Shaw JJ: **Leishmania in phlebotomid sandflies: VI. Importance of hindgut development in distinguishing between parasites of the Leishmania mexicana and L. braziliensis complexes**. *Proc R Soc Lond B Biol Sci* 1977, **199**(1135):309-320.
16. Bates PA: **Transmission of Leishmania metacyclic promastigotes by phlebotomine sand flies**. *Int J Parasitol* 2007, **37**(10):1097-1106.

17. Croft SL, Sundar S, Fairlamb AH: **Drug resistance in leishmaniasis**. *Clin Microbiol Rev* 2006, **19**(1):111-126.
18. Croft SL: **Monitoring drug resistance in leishmaniasis**. *Trop Med Int Health* 2001, **6**(11):899-905.
19. Kedzierski L, Sakthianandeswaren A, Curtis JM, Andrews PC, Junk PC, Kedzierska K: **Leishmaniasis: current treatment and prospects for new drugs and vaccines**. *Curr Med Chem* 2009, **16**(5):599-614.
20. Moore EM, Lockwood DN: **Treatment of visceral leishmaniasis**. *J Glob Infect Dis* 2009, **2**(2):151-158.
21. Moore E, O'Flaherty D, Heuvelmans H, Seaman J, Veeken H, de Wit S, Davidson RN: **Comparison of generic and proprietary sodium stibogluconate for the treatment of visceral leishmaniasis in Kenya**. *Bull World Health Organ* 2001, **79**(5):388-393.
22. Stuart K, Brun R, Croft S, Fairlamb A, Gurtler RE, McKerrow J, Reed S, Tarleton R: **Kinetoplastids: related protozoan pathogens, different diseases**. *J Clin Invest* 2008, **118**(4):1301-1310.
23. Bern C, Kjos S, Yabsley MJ, Montgomery SP: **Trypanosoma cruzi and Chagas' Disease in the United States**. *Clin Microbiol Rev* 2011, **24**(4):655-681.
24. Aguiar C, Batista AM, Pavan TB, Almeida EA, Guariento ME, Wanderley JS, Costa SC: **Serological profiles and evaluation of parasitaemia by PCR and blood culture in individuals chronically infected by Trypanosoma cruzi treated with benzonidazole**. *Trop Med Int Health*.
25. Benchimol Barbosa PR: **The oral transmission of Chagas' disease: an acute form of infection responsible for regional outbreaks**. *Int J Cardiol* 2006, **112**(1):132-133.
26. Toso MA, Vial UF, Galanti N: **Oral transmission of Chagas' disease**. *Rev Med Chil* 2011, **139**(2):258-266.
27. Yoshida N: **Molecular mechanisms of Trypanosoma cruzi infection by oral route**. *Mem Inst Oswaldo Cruz* 2009, **104 Suppl 1**:101-107.
28. Benjamin RJ, Stramer SL, Leiby DA, Dodd RY, Fearon M, Castro E: **Trypanosoma cruzi infection in North America and Spain: evidence in support of transfusion transmission**. *Transfusion* 2012.
29. Schwartz BS, Paster M, Ison MG, Chin-Hong PV: **Organ donor screening practices for Trypanosoma cruzi infection among US Organ Procurement Organizations**. *Am J Transplant* 2011, **11**(4):848-851.
30. Carlier Y, Truyens C, Deloron P, Peyron F: **Congenital parasitic infections: a review**. *Acta Trop* 2012, **121**(2):55-70.
31. Kinoshita-Yanaga AT, Toledo MJ, Araujo SM, Vier BP, Gomes ML: **Accidental infection by Trypanosoma cruzi follow-up by the polymerase chain reaction: case report**. *Rev Inst Med Trop Sao Paulo* 2009, **51**(5):295-298.
32. Paba J, Santana JM, Teixeira AR, Fontes W, Sousa MV, Ricart CA: **Proteomic analysis of the human pathogen Trypanosoma cruzi**. *Proteomics* 2004, **4**(4):1052-1059.
33. Gelb MH, Brunsveld L, Hrycyna CA, Michaelis S, Tamanoi F, Van Voorhis WC, Waldmann H: **Therapeutic intervention based on protein prenylation and associated modifications**. *Nat Chem Biol* 2006, **2**(10):518-528.
34. Russell RG: **Bisphosphonates: the first 40 years**. *Bone* 2011, **49**(1):2-19.
35. Oldfield E: **Targeting isoprenoid biosynthesis for drug discovery: bench to bedside**. *Acc Chem Res* 2010, **43**(9):1216-1226.

36. Ebetino FH, Hogan AM, Sun S, Tsoumpra MK, Duan X, Triffitt JT, Kwaasi AA, Dunford JE, Barnett BL, Oppermann U *et al*: **The relationship between the chemistry and biological activity of the bisphosphonates**. *Bone* 2011, **49**(1):20-33.
37. Artz JD, Wernimont AK, Dunford JE, Schapira M, Dong A, Zhao Y, Lew J, Russell RG, Ebetino FH, Oppermann U *et al*: **Molecular characterization of a novel geranylgeranyl pyrophosphate synthase from Plasmodium parasites**. *J Biol Chem* 2011, **286**(5):3315-3322.
38. Sun S, McKenna CE: **Farnesyl pyrophosphate synthase modulators: a patent review (2006 - 2010)**. *Expert Opin Ther Pat* 2011, **21**(9):1433-1451.
39. Yardley V, Khan AA, Martin MB, Slifer TR, Araujo FG, Moreno SN, Docampo R, Croft SL, Oldfield E: **In vivo activities of farnesyl pyrophosphate synthase inhibitors against Leishmania donovani and Toxoplasma gondii**. *Antimicrob Agents Chemother* 2002, **46**(3):929-931.
40. Ling Y, Sahota G, Odeh S, Chan JM, Araujo FG, Moreno SN, Oldfield E: **Bisphosphonate inhibitors of Toxoplasma gondi growth: in vitro, QSAR, and in vivo investigations**. *J Med Chem* 2005, **48**(9):3130-3140.
41. Kotsikorou E, Song Y, Chan JM, Faelens S, Tovian Z, Broderick E, Bakalara N, Docampo R, Oldfield E: **Bisphosphonate inhibition of the exopolyphosphatase activity of the Trypanosoma brucei soluble vacuolar pyrophosphatase**. *J Med Chem* 2005, **48**(19):6128-6139.
42. Bouzahzah B, Jelicks LA, Morris SA, Weiss LM, Tanowitz HB: **Risedronate in the treatment of Murine Chagas' disease**. *Parasitol Res* 2005, **96**(3):184-187.
43. Urbina JA, Moreno B, Vierkotter S, Oldfield E, Payares G, Sanoja C, Bailey BN, Yan W, Scott DA, Moreno SN *et al*: **Trypanosoma cruzi contains major pyrophosphate stores, and its growth in vitro and in vivo is blocked by pyrophosphate analogs**. *J Biol Chem* 1999, **274**(47):33609-33615.
44. Jordao FM, Saito AY, Miguel DC, de Jesus Peres V, Kimura EA, Katzin AM: **In vitro and in vivo antiplasmodial activities of risedronate and its interference with protein prenylation in Plasmodium falciparum**. *Antimicrob Agents Chemother* 2011, **55**(5):2026-2031.
45. Poulter CD, Argyle JC, Mash EA: **Farnesyl pyrophosphate synthetase. Mechanistic studies of the 1'-4 coupling reaction with 2-fluorogeranyl pyrophosphate**. *J Biol Chem* 1978, **253**(20):7227-7233.
46. Marrero PF, Poulter CD, Edwards PA: **Effects of site-directed mutagenesis of the highly conserved aspartate residues in domain II of farnesyl diphosphate synthase activity**. *J Biol Chem* 1992, **267**(30):21873-21878.
47. Laskovics FM, Poulter CD: **Prenyltransferase; determination of the binding mechanism and individual kinetic constants for farnesylpyrophosphate synthetase by rapid quench and isotope partitioning experiments**. *Biochemistry* 1981, **20**(7):1893-1901.
48. Song L, Poulter CD: **Yeast farnesyl-diphosphate synthase: site-directed mutagenesis of residues in highly conserved prenyltransferase domains I and II**. *Proc Natl Acad Sci U S A* 1994, **91**(8):3044-3048.
49. Joly A, Edwards PA: **Effect of site-directed mutagenesis of conserved aspartate and arginine residues upon farnesyl diphosphate synthase activity**. *J Biol Chem* 1993, **268**(36):26983-26989.

50. Koyama T, Tajima M, Nishino T, Ogura K: **Significance of Phe-220 and Gln-221 in the catalytic mechanism of farnesyl diphosphate synthase of Bacillus stearothermophilus**. *Biochem Biophys Res Commun* 1995, **212**(2):681-686.
51. Rodan GA, Martin TJ: **Therapeutic approaches to bone diseases**. *Science* 2000, **289**(5484):1508-1514.
52. Reszka AA, Halasy-Nagy JM, Masarachia PJ, Rodan GA: **Bisphosphonates act directly on the osteoclast to induce caspase cleavage of mst1 kinase during apoptosis. A link between inhibition of the mevalonate pathway and regulation of an apoptosis-promoting kinase**. *J Biol Chem* 1999, **274**(49):34967-34973.
53. Sanders JM, Song Y, Chan JM, Zhang Y, Jennings S, Kosztowski T, Odeh S, Flessner R, Schwerdtfeger C, Kotsikorou E *et al*: **Pyridinium-1-yl bisphosphonates are potent inhibitors of farnesyl diphosphate synthase and bone resorption**. *J Med Chem* 2005, **48**(8):2957-2963.
54. Rodriguez N, Bailey BN, Martin MB, Oldfield E, Urbina JA, Docampo R: **Radical cure of experimental cutaneous leishmaniasis by the bisphosphonate pamidronate**. *J Infect Dis* 2002, **186**(1):138-140.
55. Rondeau JM, Bitsch F, Bourgier E, Geiser M, Hemmig R, Kroemer M, Lehmann S, Ramage P, Rieffel S, Strauss A *et al*: **Structural basis for the exceptional in vivo efficacy of bisphosphonate drugs**. *ChemMedChem* 2006, **1**(2):267-273.
56. Tarshis LC, Yan M, Poulter CD, Sacchettini JC: **Crystal structure of recombinant farnesyl diphosphate synthase at 2.6-A resolution**. *Biochemistry* 1994, **33**(36):10871-10877.
57. Tarshis LC, Proteau PJ, Kellogg BA, Sacchettini JC, Poulter CD: **Regulation of product chain length by isoprenyl diphosphate synthases**. *Proc Natl Acad Sci U S A* 1996, **93**(26):15018-15023.
58. Kavanagh KL, Guo K, Dunford JE, Wu X, Knapp S, Ebetino FH, Rogers MJ, Russell RG, Oppermann U: **The molecular mechanism of nitrogen-containing bisphosphonates as antiosteoporosis drugs**. *Proc Natl Acad Sci U S A* 2006, **103**(20):7829-7834.
59. Ohnuma S, Narita K, Nakazawa T, Ishida C, Takeuchi Y, Ohto C, Nishino T: **A role of the amino acid residue located on the fifth position before the first aspartate-rich motif of farnesyl diphosphate synthase on determination of the final product**. *J Biol Chem* 1996, **271**(48):30748-30754.
60. John R. Baker RMaDR: **Advances in Parasitology**, vol. 64; 2007.
61. Narita K, Ohnuma S, Nishino T: **Protein design of geranyl diphosphate synthase. Structural features that define the product specificities of prenyltransferases**. *J Biochem* 1999, **126**(3):566-571.
62. Szkopinska A, Plochocka D: **Farnesyl diphosphate synthase; regulation of product specificity**. *Acta Biochim Pol* 2005, **52**(1):45-55.
63. Montalvetti A, Fernandez A, Sanders JM, Ghosh S, Van Brussel E, Oldfield E, Docampo R: **Farnesyl pyrophosphate synthase is an essential enzyme in Trypanosoma brucei. In vitro RNA interference and in vivo inhibition studies**. *J Biol Chem* 2003, **278**(19):17075-17083.
64. Urbina JA, Docampo R: **Specific chemotherapy of Chagas disease: controversies and advances**. *Trends Parasitol* 2003, **19**(11):495-501.
65. WHO: *wwwwhoint/topics/tropical_diseases/en/*.
66. Brener Z: **Biology of Trypanosoma cruzi**. *Annu Rev Microbiol* 1973, **27**:347-382.

67. Kirchhoff LV: **American trypanosomiasis (Chagas' disease)--a tropical disease now in the United States**. *N Engl J Med* 1993, **329**(9):639-644.
68. Galel SA, Kirchhoff LV: **Risk factors for Trypanosoma cruzi infection in California blood donors**. *Transfusion* 1996, **36**(3):227-231.
69. Urbina JA: **Specific chemotherapy of Chagas disease: relevance, current limitations and new approaches**. *Acta Trop* 2010, **115**(1-2):55-68.
70. Roelofs AJ, Thompson K, Ebetino FH, Rogers MJ, Coxon FP: **Bisphosphonates: molecular mechanisms of action and effects on bone cells, monocytes and macrophages**. *Curr Pharm Des* 2010, **16**(27):2950-2960.
71. Reszka AA, Rodan GA: **Nitrogen-containing bisphosphonate mechanism of action**. *Mini Rev Med Chem* 2004, **4**(7):711-719.
72. Russell RG, Rogers MJ: **Bisphosphonates: from the laboratory to the clinic and back again**. *Bone* 1999, **25**(1):97-106.
73. Reszka AA, Rodan GA: **Mechanism of action of bisphosphonates**. *Curr Osteoporos Rep* 2003, **1**(2):45-52.
74. Fleisch H, Russell RG, Straumann F: **Effect of pyrophosphate on hydroxyapatite and its implications in calcium homeostasis**. *Nature* 1966, **212**(5065):901-903.
75. Fleisch H, Russell RG, Francis MD: **Diphosphonates inhibit hydroxyapatite dissolution in vitro and bone resorption in tissue culture and in vivo**. *Science* 1969, **165**(3899):1262-1264.
76. Francis MD, Russell RG, Fleisch H: **Diphosphonates inhibit formation of calcium phosphate crystals in vitro and pathological calcification in vivo**. *Science* 1969, **165**(3899):1264-1266.
77. Hughes DE, Wright KR, Uy HL, Sasaki A, Yoneda T, Roodman GD, Mundy GR, Boyce BF: **Bisphosphonates promote apoptosis in murine osteoclasts in vitro and in vivo**. *J Bone Miner Res* 1995, **10**(10):1478-1487.
78. Rogers MJ, Frith JC, Luckman SP, Coxon FP, Benford HL, Monkkonen J, Auriola S, Chilton KM, Russell RG: **Molecular mechanisms of action of bisphosphonates**. *Bone* 1999, **24**(5 Suppl):73S-79S.
79. Hosfield DJ, Zhang Y, Dougan DR, Broun A, Tari LW, Swanson RV, Finn J: **Structural basis for bisphosphonate-mediated inhibition of isoprenoid biosynthesis**. *J Biol Chem* 2004, **279**(10):8526-8529.
80. Cheng F, Oldfield E: **Inhibition of isoprene biosynthesis pathway enzymes by phosphonates, bisphosphonates, and diphosphates**. *J Med Chem* 2004, **47**(21):5149-5158.
81. Dunford JE, Thompson K, Coxon FP, Luckman SP, Hahn FM, Poulter CD, Ebetino FH, Rogers MJ: **Structure-activity relationships for inhibition of farnesyl diphosphate synthase in vitro and inhibition of bone resorption in vivo by nitrogen-containing bisphosphonates**. *J Pharmacol Exp Ther* 2001, **296**(2):235-242.
82. van Beek E, Pieterman E, Cohen L, Lowik C, Papapoulos S: **Farnesyl pyrophosphate synthase is the molecular target of nitrogen-containing bisphosphonates**. *Biochem Biophys Res Commun* 1999, **264**(1):108-111.
83. Coxon FP, Thompson K, Rogers MJ: **Recent advances in understanding the mechanism of action of bisphosphonates**. *Curr Opin Pharmacol* 2006, **6**(3):307-312.

84. Sanders JM, Ghosh S, Chan JM, Meints G, Wang H, Raker AM, Song Y, Colantino A, Burzynska A, Kafarski P *et al*: **Quantitative structure-activity relationships for gammadelta T cell activation by bisphosphonates**. *J Med Chem* 2004, **47**(2):375-384.
85. Reddy R, Dietrich E, Lafontaine Y, Houghton TJ, Belanger O, Dubois A, Arhin FF, Sarmiento I, Fadhil I, Laquerre K *et al*: **Bisphosphonated benzoxazinorifamycin prodrugs for the prevention and treatment of osteomyelitis**. *ChemMedChem* 2008, **3**(12):1863-1868.
86. Forlani G, Giberti S, Berlicki L, Petrollino D, Kafarski P: **Plant P5C reductase as a new target for aminomethylenebisphosphonates**. *J Agric Food Chem* 2007, **55**(11):4340-4347.
87. Clezardin P, Massaia M: **Nitrogen-containing bisphosphonates and cancer immunotherapy**. *Curr Pharm Des* 2010, **16**(27):3007-2014.
88. Miller K, Erez R, Segal E, Shabat D, Satchi-Fainaro R: **Targeting bone metastases with a bispecific anticancer and antiangiogenic polymer-alendronate-taxane conjugate**. *Angew Chem Int Ed Engl* 2009, **48**(16):2949-2954.
89. Zhang Y, Cao R, Yin F, Hudock MP, Guo RT, Krysiak K, Mukherjee S, Gao YG, Robinson H, Song Y *et al*: **Lipophilic bisphosphonates as dual farnesyl/geranylgeranyl diphosphate synthase inhibitors: an X-ray and NMR investigation**. *J Am Chem Soc* 2009, **131**(14):5153-5162.
90. Coleman RE: **Risks and benefits of bisphosphonates**. *Br J Cancer* 2008, **98**(11):1736-1740.
91. Docampo R, Moreno SN: **The acidocalcisome as a target for chemotherapeutic agents in protozoan parasites**. *Curr Pharm Des* 2008, **14**(9):882-888.
92. Ghosh S, Chan JM, Lea CR, Meints GA, Lewis JC, Tovian ZS, Flessner RM, Loftus TC, Bruchhaus I, Kendrick H *et al*: **Effects of bisphosphonates on the growth of Entamoeba histolytica and Plasmodium species in vitro and in vivo**. *J Med Chem* 2004, **47**(1):175-187.
93. Martin MB, Grimley JS, Lewis JC, Heath HT, 3rd, Bailey BN, Kendrick H, Yardley V, Caldera A, Lira R, Urbina JA *et al*: **Bisphosphonates inhibit the growth of Trypanosoma brucei, Trypanosoma cruzi, Leishmania donovani, Toxoplasma gondii, and Plasmodium falciparum: a potential route to chemotherapy**. *J Med Chem* 2001, **44**(6):909-916.
94. Martin MB, Sanders JM, Kendrick H, de Luca-Fradley K, Lewis JC, Grimley JS, Van Brussel EM, Olsen JR, Meints GA, Burzynska A *et al*: **Activity of bisphosphonates against Trypanosoma brucei rhodesiense**. *J Med Chem* 2002, **45**(14):2904-2914.
95. Rosso VS, Szajnman SH, Malayil L, Galizzi M, Moreno SN, Docampo R, Rodriguez JB: **Synthesis and biological evaluation of new 2-alkylaminoethyl-1,1-bisphosphonic acids against Trypanosoma cruzi and Toxoplasma gondii targeting farnesyl diphosphate synthase**. *Bioorg Med Chem* 2011, **19**(7):2211-2217.
96. Szajnman SH, Bailey BN, Docampo R, Rodriguez JB: **Bisphosphonates derived from fatty acids are potent growth inhibitors of Trypanosoma cruzi**. *Bioorg Med Chem Lett* 2001, **11**(6):789-792.
97. Szajnman SH, Garcia Linares GE, Li ZH, Jiang C, Galizzi M, Bontempi EJ, Ferella M, Moreno SN, Docampo R, Rodriguez JB: **Synthesis and biological evaluation of 2-alkylaminoethyl-1,1-bisphosphonic acids against Trypanosoma cruzi and Toxoplasma gondii targeting farnesyl diphosphate synthase**. *Bioorg Med Chem* 2008, **16**(6):3283-3290.

98. Szajnman SH, Montalvetti A, Wang Y, Docampo R, Rodriguez JB: **Bisphosphonates derived from fatty acids are potent inhibitors of Trypanosoma cruzi farnesyl pyrophosphate synthase**. *Bioorg Med Chem Lett* 2003, **13**(19):3231-3235.
99. Szajnman SH, Ravaschino EL, Docampo R, Rodriguez JB: **Synthesis and biological evaluation of 1-amino-1,1-bisphosphonates derived from fatty acids against Trypanosoma cruzi targeting farnesyl pyrophosphate synthase**. *Bioorg Med Chem Lett* 2005, **15**(21):4685-4690.
100. Laskovics FM, Krafcik JM, Poulter CD: **Prenyltransferase. Kinetic studies of the 1'-4 coupling reaction with avian liver enzyme**. *J Biol Chem* 1979, **254**(19):9458-9463.
101. Ding VD, Sheares BT, Bergstrom JD, Ponpipom MM, Perez LB, Poulter CD: **Purification and characterization of recombinant human farnesyl diphosphate synthase expressed in Escherichia coli**. *Biochem J* 1991, **275 (Pt 1)**:61-65.
102. Ohnuma S, Nakazawa T, Hemmi H, Hallberg AM, Koyama T, Ogura K, Nishino T: **Conversion from farnesyl diphosphate synthase to geranylgeranyl diphosphate synthase by random chemical mutagenesis**. *J Biol Chem* 1996, **271**(17):10087-10095.
103. Ortiz-Gomez A, Jimenez C, Estevez AM, Carrero-Lerida J, Ruiz-Perez LM, Gonzalez-Pacanowska D: **Farnesyl diphosphate synthase is a cytosolic enzyme in Leishmania major promastigotes and its overexpression confers resistance to risedronate**. *Eukaryot Cell* 2006, **5**(7):1057-1064.
104. Jancarik J, Kim SH: **Sparse-Matrix Sampling - a Screening Method for Crystallization of Proteins**. *J Appl Crystallogr* 1991, **24**:409-411.
105. Otwinowski Z, Minor W: **Processing of X-ray diffraction data collected in oscillation mode**. *Macromolecular Crystallography, Pt A* 1997, **276**:307-326.
106. Navaza J: **Amore - an Automated Package for Molecular Replacement**. *Acta Crystallogr A* 1994, **50**:157-163.
107. Jones TA, Zou JY, Cowan SW, Kjeldgaard M: **Improved Methods for Building Protein Models in Electron-Density Maps and the Location of Errors in These Models**. *Acta Crystallogr A* 1991, **47**:110-119.
108. Winn MD, Isupov MN, Murshudov GN: **Use of TLS parameters to model anisotropic displacements in macromolecular refinement**. *Acta Crystallogr D* 2001, **57**:122-133.
109. Murshudov GN, Skubak P, Lebedev AA, Pannu NS, Steiner RA, Nicholls RA, Winn MD, Long F, Vagin AA: **REFMAC5 for the refinement of macromolecular crystal structures**. *Acta Crystallogr D* 2011, **67**:355-367.
110. Winn MD, Ballard CC, Cowtan KD, Dodson EJ, Emsley P, Evans PR, Keegan RM, Krissinel EB, Leslie AG, McCoy A *et al*: **Overview of the CCP4 suite and current developments**. *Acta Crystallogr D Biol Crystallogr* 2011, **67**(Pt 4):235-242.
111. Emsley P, Lohkamp B, Scott WG, Cowtan K: **Features and development of Coot**. *Acta Crystallogr D* 2010, **66**:486-501.
112. Laskowski RA, Macarthur MW, Moss DS, Thornton JM: **Procheck - a Program to Check the Stereochemical Quality of Protein Structures**. *J Appl Crystallogr* 1993, **26**:283-291.
113. Hooft RW, Vriend G, Sander C, Abola EE: **Errors in protein structures**. *Nature* 1996, **381**(6580):272.
114. Hooft RWW, Sander C, Vriend G: **Verification of protein structures: Side-chain planarity**. *J Appl Crystallogr* 1996, **29**:714-716.
115. Kraulis PJ: **Molscript - a Program to Produce Both Detailed and Schematic Plots of Protein Structures**. *J Appl Crystallogr* 1991, **24**:946-950.

116. Cunningham B: **Protective effects of colostral antibodies to Br abortus on strain 19 vaccination and field injection**. *Vet Rec* 1977, **101**(26-27):521-524.
117. Cunningham JJ, Jackson DV, Jr.: **Lymphographic and echographic findings in angioimmunoblastic lymphadenopathy**. *Arch Intern Med* 1977, **137**(12):1693-1695.
118. Szajnman SH, Linares GG, Moro P, Rodriguez JB: **New insights into the chemistry of gem-bis(phosphonates): Unexpected rearrangement of Michael-type acceptors**. *Eur J Org Chem* 2005(17):3687-3696.
119. Degenhardt CR, Burdsall DC: **Synthesis of Ethenylidenebis(Phosphonic Acid) and Its Tetraalkyl Esters**. *Journal of Organic Chemistry* 1986, **51**(18):3488-3490.
120. Lazzarato L, Rolando B, Lolli ML, Tron GC, Fruttero R, Gasco A, Deleide G, Guenther HL: **Synthesis of NO-donor bisphosphonates and their in-vitro action on bone resorption**. *J Med Chem* 2005, **48**(5):1322-1329.
121. Huang CH, Gabelli SB, Oldfield E, Amzel LM: **Binding of nitrogen-containing bisphosphonates (N-BPs) to the Trypanosoma cruzi farnesyl diphosphate synthase homodimer**. *Proteins*, **78**(4):888-899.
122. Bailey S: **The Ccp4 Suite - Programs for Protein Crystallography**. *Acta Crystallogr D* 1994, **50**:760-763.
123. Allaire M YL: **Biomolecular solution X-ray scattering at the National Synchrotron Light Source**. *J Synchrotron Radiat* 2011, **18**:41-44.
124. Konarev PV VV, Sokolova AV, Koch MHJ, Svergun DI: **PRIMUS: a Windows PC-based system for small-angle scattering data analysis.** *J Appl Crystallogr* 2003, **36**:1277-1282.
125. Allaire M, Yang L: **Biomolecular solution X-ray scattering at the National Synchrotron Light Source**. *J Synchrotron Radiat* 2011, **18**(1):41-44.
126. DI S: **Determination of the Regularization Parameter in Indirect-Transform Methods Using Perceptual Criteria.** *J Appl Crystallogr* 1992, **25**:495-503.
127. Svergun D BC, Koch MHJ: **CRYSOL - a Program to Evaluate X-ray Solution Scattering of Biological Macromolecules from Atomic Coordinates. Journal of Applied Crystallography**. 1995, **28**:768-773.
128. Franke D SD: **DAMMIF, a program for rapid ab-initio shape determination in small-angle scattering.** *J Appl Crystallogr* 2009, **42**:342-346.
129. Kozin MB SD: **A software system for rigid-body modelling of solution scattering data.** . *J Appl Crystallogr*, **33**:775-777.
130. Ferella M, Montalvetti A, Rohloff P, Miranda K, Fang J, Reina S, Kawamukai M, Bua J, Nilsson D, Pravia C *et al*: **A solanesyl-diphosphate synthase localizes in glycosomes of Trypanosoma cruzi**. *J Biol Chem* 2006, **281**(51):39339-39348.

Vita

Srinivas Aripirala

Email: saripir1@jhu.edu
Phone: (410)-868-1123
Address: 725 N. Wolfe Street
WBSB 605, Baltimore, MD 21205

EDUCATION

Johns Hopkins University, Baltimore, MD, USA **2006-2013**
PhD in Biophysics & Biophysical Chemistry

Indian Institute of Technology, Kharagpur, WB, India **1999-2004**
Integrated MSc in Mathematics & Computing

RESEARCH EXPERIENCE

Johns Hopkins University, Baltimore, MD: *Graduate Student Researcher* **2007 –**

- Structural and thermodynamic characterization of *Leishmania major* Farnesyl diphosphate synthase, a key enzyme in the mevalonate pathway producing compounds of chain length C15
- Expression, purification and thermodynamic analysis of Trypanosoma cruzi Solanesyl diphoshphate synthase, E- polyprenyl diphosphate synthase producing compounds of chain length C45
- Design, synthesis and thermodynamic characterization of the interaction between the new class of drugs 1-alkylamino bisphosphonates and Trypanasoma cruzi Farnesyl diphosphate synthase
- Site directed mutagenesis studies of Leishmania major Farnesyl disphosphate synthase to produce a mixture of GPP and FPP
- Thermodynamic characterization of the interaction between $Na_v1.5$ and Calmodulin

PUBLICATIONS

- Aripirala S, Szajnman SH, Jakoncic J, Kaiser M, Gabelli SB, Amzel LM: Design, synthesis, calorimetry, and crystallographic analysis of 2-alkylaminoethyl-1,1-bisphosphonates as inhibitors of Trypanosoma cruzi farnesyl diphosphate synthase. J Med Chem 2012, 55(14):6445-6454.

- Aripirala S, Dolores GP, Oldfield E, Docampo R, Amzel LM, Gabelli SB: Structural and thermodynamic basis of the inhibition of *Leishmania major* Farnesyl Diphosphate Synthase by nitrogen containing bisphosphonates (Accepted in Acta Crystallographica D)

- Aripirala S, Kim YS, Gabelli SB, Amzel LM: Genetic engineering of Leishmania major Farnesyl diphosphate synthase to produce a mixture of Geranyl diphosphate and Farnesyl disphosphate (manuscript in preparation)

- Moreira DC, Aripirala S, Gabelli SB, Amzel LM: Farnesyl diphosphate synthases as targets for antiparasitic drug design. (Review under preparation)

POSTERS & PRESENTATIONS

- Design, Synthesis, Calorimetry and Crystallographic analysis of 2-Alkylaminoethyl-1,1-Bisphosphonates as inhibitors of Trypanosoma cruzi Farnesyl Diphosphate Synthase. Poster. ACA, Boston **2012**
- Structural Insights into the enzymes of the Mevalonate pathway in Trypanosomatids. Poster. Institute for Biophysical Research Retreat. **2011**
- Inhibitors of Leishmania major Farnesyl Diphosphate Synthase: Crystallographic and Calorimetric studies. Poster. Biophysical Society meeting. Baltimore **2011**
- Leishmania major Farnesyl Diphosphate Synthase: Structure Determination and Comparison with its human ortholog. Poster. Institute for Biophysical Research Retreat. **2009**

MENTORING EXPERIENCE

- Yu-Seon Kim, Undergraduate, Johns Hopkins University
- Aisha Davis, Medical school student, Indiana University School of Medicine

TECHNIQUES

Molecular Biology

Cloning, PCR, Site-directed Mutagenesis, Gel Electrophoresis, Western Blot Analysis

Protein Expression, Protein Purification

Affinity Chromatography, Ion-exchange Chromatography, Size-exclusion Chromatography, Ammonium Sulfate Precipitation, HPLC

Protein Characterization

Thermal-shift Assay, Isothermal Titration Calorimetry, Protein X-ray Crystallography, Small Angle X-ray Scattering for Proteins, Enzymatic Assay, Reaction Kinetics Inhibition, Colorimetric & Coupled assay

Molecular Modeling

Homology Modeling, Docking, Molecular Dynamics Simulation

Software:
Molecular Modeling: QUANTA, MOE AUTODOCK
Crystallography: O, Coot, CNS, CCP4 suite, HKL2000
Molecular Dynamics: CHARMM, NAMD
Molecular Visualization: PYMOL, VMD, Molscript

AWARDS AND AFFILIATIONS

- Recipient of **Travel Award** for the American Crystallographic Association conference **2012**
- Recipient of Fellowship from the Department of Energy **2006 - 2008**
- Member of American Crystallographic Association **2012 - 2013**
- Member of Biophysics Society **2010 - 2012**